

Supplementary Information: Phosphorus and transition metal segregation in iron grain boundaries from first principles

Han Lin Mai ^{1,a}, Xiang-Yuan Cui ^{2,a}, Daniel Scheiber ^{3,b}, Lorenz Romaner ^{4,c},
Simon P. Ringer ^{5,a}

^a*The University of Sydney, Faculty of Engineering, School of Aerospace, Mechanical and Mechatronic Engineering & Australian Centre for Microscopy and Microanalysis, 2006 New South Wales, Australia*

^b*Materials Center Leoben Forschung GmbH, Roseggerstraße 12, 8700 Leoben, Austria*

^c*Department of Materials Science, University of Leoben, Franz-Josefstraße 18, 8700 Leoben, Austria.*

1. Convergence tests

We refer readers to the Supplementary Information (S.I.) of our previous paper for extensive convergence tests for the four model GBs studied here [1].

2. Cells with vacuum

Aside from the GB energy and excess volume calculations, all other calculations were conducted on cells with vacuum included. Here we present the atomic structures of the cells including vacuum:

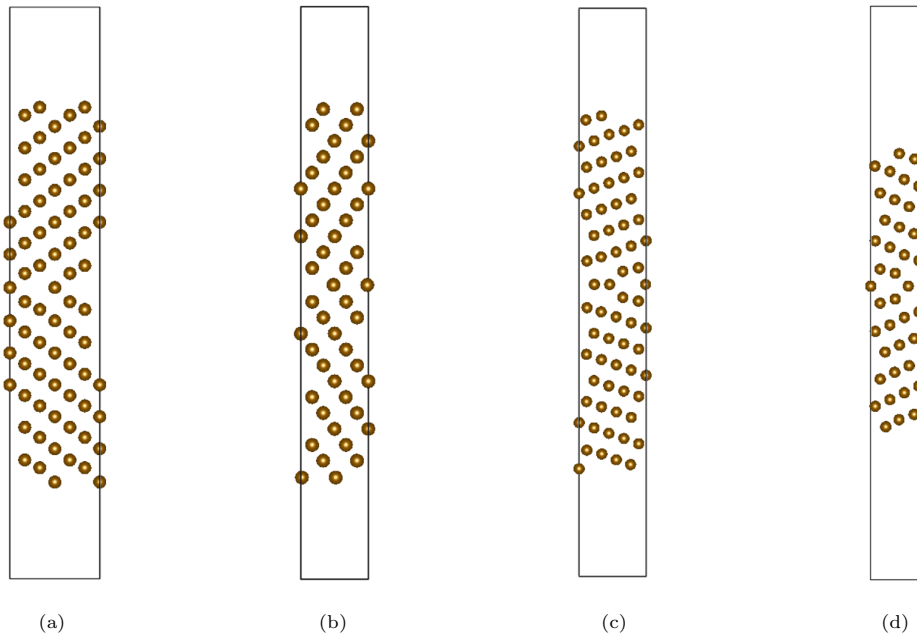


Figure S1: The atomic structures of the four characteristic model GBs studied, in the cells with vacuum included. The structures of the S1a $\Sigma_3[110](111)$, S1b $\Sigma_3[110](\bar{1}\bar{1}2)$, S1c $\Sigma_9[110](\bar{2}\bar{2}1)$ and the S1d $\Sigma_{11}[110](3\bar{3}2)$ GBs, respectively. The dimensions of these cells are given in Table 1 in the main text.

¹han.mai@sydney.edu.au

²carl.cui@sydney.edu.au

³daniel.scheiber@mcl.at

⁴lorenz.romaner@unileoben.ac.at

⁵simon.ringer@sydney.edu.au

3. Structure files (GB+vac)

We provide the base structure files that were modified in the study to generate the various structures. Please note that the sites in all following Tables (often given as a number in the “system” columns) in the S.I. are zero-indexed. i.e. the first site is denoted as site 0. For incremental segregation, one must first fully relax the structure with the prior segregant completely before adding the secondary segregant to reproduce our results exactly.

3.1. $\Sigma 3[110](1\bar{1}1)$

GB-S3-RA110-S1-11.vasp

```
Fe72
1.0
4.004839 0.000000 0.000000
0.000000 6.936585 0.000000
0.000000 0.000000 44.144156
Fe
72
direct
0.500020 0.499865 0.174406 Fe
0.000020 0.999864 0.174406 Fe
0.000018 0.333206 0.192023 Fe
0.500018 0.833206 0.192023 Fe
0.000016 0.666432 0.207212 Fe
0.500016 0.166432 0.207212 Fe
0.500017 0.499846 0.227842 Fe
0.000018 0.999846 0.227842 Fe
0.000006 0.333167 0.246510 Fe
0.500006 0.833169 0.246511 Fe
0.500004 0.166563 0.264928 Fe
0.000002 0.666564 0.264928 Fe
0.499996 0.499844 0.283536 Fe
0.999996 0.999844 0.283536 Fe
0.999992 0.333274 0.302182 Fe
0.499992 0.833274 0.302182 Fe
0.999988 0.666648 0.320456 Fe
0.499987 0.166648 0.320456 Fe
0.499986 0.499993 0.339148 Fe
0.999986 -0.000007 0.339148 Fe
0.499982 0.833339 0.357718 Fe
0.999982 0.333339 0.357718 Fe
0.999982 0.666700 0.376090 Fe
0.499982 0.166698 0.376090 Fe
0.999978 0.000108 0.395020 Fe
```

0.499977 0.500108 0.395020 Fe
0.499980 0.833452 0.413457 Fe
0.999981 0.333452 0.413457 Fe
0.999980 0.666854 0.431511 Fe
0.499980 0.166855 0.431511 Fe
0.999981 0.000060 0.451243 Fe
0.499981 0.500060 0.451243 Fe
0.499979 0.833396 0.471109 Fe
0.999979 0.333396 0.471109 Fe
0.999978 0.666829 0.484584 Fe
0.499978 0.166829 0.484584 Fe
0.999998 0.000365 0.509449 Fe
0.499999 0.500365 0.509449 Fe
0.500023 0.166916 0.534317 Fe
0.000023 0.666916 0.534317 Fe
0.000025 0.333423 0.547997 Fe
0.500025 0.833423 0.547997 Fe
0.000026 0.000056 0.567672 Fe
0.500026 0.500056 0.567672 Fe
0.000029 0.666838 0.587404 Fe
0.500029 0.166838 0.587404 Fe
0.500033 0.833415 0.605344 Fe
0.000032 0.333415 0.605344 Fe
0.000036 0.000019 0.623791 Fe
0.500036 0.500018 0.623791 Fe
0.500038 0.166680 0.642703 Fe
0.000038 0.666680 0.642703 Fe
0.000047 0.333340 0.661100 Fe
0.500047 0.833340 0.661100 Fe
0.000044 0.999937 0.679572 Fe
0.500044 0.499937 0.679572 Fe
0.000046 0.666642 0.697998 Fe
0.500046 0.166642 0.697998 Fe
0.500051 0.833194 0.716553 Fe
0.000051 0.333194 0.716553 Fe
0.500050 0.499867 0.735116 Fe
0.000050 0.999867 0.735116 Fe
0.500050 0.166530 0.753562 Fe
0.000050 0.666530 0.753562 Fe
0.500048 0.833172 0.772186 Fe
0.000048 0.333172 0.772186 Fe
0.000046 0.999749 0.792716 Fe
0.500046 0.499749 0.792716 Fe
0.000049 0.666488 0.808004 Fe

```
0.500049 0.166488 0.808004 Fe  
0.500049 0.833140 0.825542 Fe  
0.000049 0.333140 0.825542 Fe
```

3.2. $\Sigma 3[110](1\bar{1}2)$

GB-S3-RA110-S1-12.vasp

```
Fe48  
1.0  
4.004839 0.000000 0.000000  
0.000000 4.904906 0.000000  
0.000000 0.000000 41.619509  
Fe  
48  
direct  
-0.000032 0.027731 0.179833 Fe  
-0.000032 0.527732 0.179833 Fe  
0.500066 0.330676 0.205695 Fe  
0.500066 0.830675 0.205695 Fe  
0.000005 0.168711 0.234560 Fe  
0.000005 0.668711 0.234560 Fe  
0.500017 0.500595 0.262485 Fe  
0.500017 0.000595 0.262485 Fe  
-0.000023 0.333753 0.290612 Fe  
-0.000023 0.833754 0.290612 Fe  
0.500018 0.165697 0.317980 Fe  
0.500018 0.665697 0.317980 Fe  
0.999983 0.498031 0.345981 Fe  
0.999983 0.998031 0.345981 Fe  
0.499932 0.335133 0.373491 Fe  
0.499932 0.835132 0.373491 Fe  
0.999980 0.169691 0.401247 Fe  
0.999980 0.669691 0.401247 Fe  
0.499977 0.001296 0.429178 Fe  
0.499977 0.501295 0.429178 Fe  
0.000013 0.332012 0.456982 Fe  
0.000013 0.832012 0.456982 Fe  
0.499943 0.173351 0.484747 Fe  
0.499943 0.673351 0.484747 Fe  
0.000005 0.478358 0.514052 Fe  
0.000005 0.978358 0.514052 Fe  
0.499978 0.156569 0.543367 Fe  
0.499978 0.656569 0.543367 Fe
```

```

0.000034 0.323860 0.570679 Fe
0.000034 0.823860 0.570679 Fe
0.499971 0.994852 0.598815 Fe
0.499971 0.494852 0.598815 Fe
0.999977 0.164339 0.626496 Fe
0.999977 0.664339 0.626496 Fe
0.499976 0.328743 0.654032 Fe
0.499976 0.828743 0.654032 Fe
0.000013 0.495850 0.682007 Fe
0.000013 0.995849 0.682007 Fe
0.499934 0.163876 0.709478 Fe
0.499934 0.663876 0.709478 Fe
0.000012 0.331414 0.737716 Fe
0.000012 0.831414 0.737716 Fe
0.499951 0.500704 0.765667 Fe
0.499951 0.000703 0.765667 Fe
-0.000005 0.163737 0.794539 Fe
-0.000005 0.663737 0.794539 Fe
0.499954 0.360342 0.820358 Fe
0.499954 0.860342 0.820358 Fe

```

3.3. Σ9[110](2̄21)

----- GB-S9-RA110-S2-21.vasp -----

```

Fe68
1.0
6.332207 0.000000 0.000000
-1.266441 3.799324 0.000000
0.000000 0.000000 50.973280

Fe
68
direct
0.999045 0.999514 0.189665 Fe
0.231863 0.615976 0.196912 Fe
0.445707 0.222842 0.205355 Fe
0.660958 0.830526 0.215698 Fe
0.884769 0.442348 0.222456 Fe
0.110202 0.055121 0.233555 Fe
0.331535 0.665765 0.242946 Fe
0.555275 0.277631 0.252001 Fe
0.776844 0.888408 0.261475 Fe
0.998191 0.499094 0.270686 Fe
0.221423 0.110718 0.280009 Fe

```

0.443317 0.721667 0.289373 Fe
0.665796 0.332891 0.298512 Fe
0.887979 0.943983 0.307773 Fe
0.110199 0.555101 0.316974 Fe
0.332363 0.166208 0.326200 Fe
0.554929 0.777426 0.335458 Fe
0.777528 0.388775 0.344735 Fe
0.000206 0.000085 0.353914 Fe
0.222501 0.611241 0.363265 Fe
0.444592 0.222307 0.372454 Fe
0.666790 0.833362 0.381674 Fe
0.888857 0.444427 0.390951 Fe
0.111561 0.055762 0.400131 Fe
0.334512 0.667264 0.409527 Fe
0.556405 0.278198 0.418971 Fe
0.776694 0.888374 0.427891 Fe
0.000841 0.500410 0.437235 Fe
0.223529 0.111799 0.446434 Fe
0.447145 0.723595 0.456952 Fe
0.670530 0.335247 0.465663 Fe
0.881461 0.940748 0.472993 Fe
0.115221 0.557617 0.484620 Fe
0.346684 0.173301 0.491119 Fe
0.543305 0.771682 0.513929 Fe
0.772178 0.386089 0.514015 Fe
0.008169 0.004080 0.514027 Fe
0.346789 0.173355 0.536921 Fe
0.115316 0.557683 0.543410 Fe
0.881889 0.940921 0.555063 Fe
0.670859 0.335442 0.562389 Fe
0.447455 0.723782 0.571038 Fe
0.223820 0.111947 0.581603 Fe
0.000901 0.500458 0.590801 Fe
0.776556 0.888269 0.600127 Fe
0.556264 0.278101 0.609023 Fe
0.334510 0.667238 0.618448 Fe
0.111508 0.055710 0.627800 Fe
0.888951 0.444463 0.636977 Fe
0.666704 0.833338 0.646281 Fe
0.444124 0.222092 0.655517 Fe
0.221594 0.610793 0.664713 Fe
0.999074 0.999552 0.674072 Fe
0.776539 0.388265 0.683291 Fe
0.554199 0.777068 0.692483 Fe

```

0.332013 0.166019 0.701752 Fe
0.109710 0.554847 0.710830 Fe
0.887599 0.943799 0.720219 Fe
0.664344 0.332192 0.729548 Fe
0.442912 0.721471 0.738785 Fe
0.221381 0.110702 0.748245 Fe
0.997457 0.498705 0.757259 Fe
0.776075 0.888023 0.766685 Fe
0.550889 0.275421 0.777811 Fe
0.326843 0.663460 0.784560 Fe
0.111588 0.055764 0.794857 Fe
0.898051 0.449055 0.803355 Fe
0.664982 0.832485 0.810592 Fe

```

3.4. Σ11[110](3̄3̄2)

GB-S11-RA110-S3-32.vasp

```

Fe42
1.0
4.004839 0.000000 0.000000
0.000000 4.696090 0.000000
0.000000 0.000000 50.973280

Fe
42
direct
0.999991 0.996402 0.257247 Fe
0.499991 0.287613 0.266648 Fe
0.999988 0.535670 0.279054 Fe
0.499992 0.819555 0.288320 Fe
0.999992 0.088682 0.302353 Fe
0.499990 0.364430 0.314026 Fe
0.999986 0.635970 0.326103 Fe
0.499987 0.908944 0.337639 Fe
0.999988 0.181301 0.349768 Fe
0.499989 0.453485 0.361613 Fe
0.999990 0.726869 0.373345 Fe
0.499985 0.999247 0.385282 Fe
0.999984 0.272829 0.396931 Fe
0.499987 0.545193 0.409115 Fe
0.999989 0.819193 0.420656 Fe
0.499986 0.090191 0.433033 Fe
0.999991 0.364313 0.444113 Fe
0.499992 0.636025 0.457310 Fe

```

```

0.999987 0.911096 0.467260 Fe
0.499981 0.179510 0.482203 Fe
0.999982 0.463645 0.489470 Fe
0.999979 0.005866 0.511941 Fe
0.499979 0.709611 0.511954 Fe
0.999974 0.464078 0.534358 Fe
0.499975 0.179113 0.541604 Fe
0.999964 0.911575 0.556557 Fe
0.499972 0.636340 0.566458 Fe
0.999973 0.364284 0.579712 Fe
0.499972 0.089837 0.590882 Fe
0.999969 0.818729 0.603272 Fe
0.499969 0.544535 0.614838 Fe
0.999976 0.272244 0.626893 Fe
0.499968 0.998901 0.638550 Fe
0.999968 0.726829 0.650513 Fe
0.499968 0.453366 0.662550 Fe
0.999978 0.180895 0.674263 Fe
0.499980 0.909352 0.686263 Fe
0.999978 0.633459 0.697929 Fe
0.499969 0.364764 0.711993 Fe
0.999973 0.080692 0.721253 Fe
0.499967 0.832773 0.733623 Fe
0.999971 0.541577 0.743107 Fe

```

4. Γ surface shift results

Below are the results for the gamma-shift surface described in the main text.

5. Single solute segregation

5.1. Interstitial P segregation testing

As mentioned in the main text, we extensively considered a set of interstitial positions for P in all four GBs. The positions of these interstitial sites and their corresponding segregation energies are tabulated in Tables S2-S5. For visualisation, we provide all tested starting interstitial positions in fractional coordinates for each GB in Fig. S2 (append to the given POSCARs above). These positions were selected using the interstitial finding algorithm implemented in pymatgen, InFiT. In the $\Sigma 9(2\bar{2}1)$ and $\Sigma 11(3\bar{3}2)$ GBs, we observe that the interstitial segregation of P is predicted to be strong in many cases, but this is in fact a result of a relaxation back into a substitutional-equivalent site, as mentioned in the text. We have carefully visualised and analysed all the final

relaxed structures that yielded substantially negative segregation energies. All such cases in the $\Sigma 9(2\bar{2}1)$ and $\Sigma 11(3\bar{3}2)$ GBs were found to be a case of this relaxation back into a substitutional position [examples given in Figs. S3 and S4, respectively].

a-shift	b-shift	$\Sigma 3(1\bar{1}1)$	$\Sigma 3(1\bar{1}2)$	$\Sigma 9(2\bar{2}1)$	$\Sigma 11(3\bar{3}2)$
0	0	-581.29	-388.94	-549.72	-338.11
0	0.1	-579.98	-388.64	-549.469	-338.01
0	0.2	-577.66	-388.55	-548.93	-337.26
0	0.3	-564.01	-388.29	-548.35	-336.14
0	0.4	-564.90*	-388.58	-547.93	-335.40
0	0.5	-577.92	-388.94	-547.79	-335.10
0.1	0	-580.95	-388.23	-549.28	-337.91
0.1	0.1	-579.96	-388.07	-549.28	-337.82
0.1	0.2	-577.76	-387.89	-549.02	-337.16
0.1	0.3	-563.28*	-387.48	-548.71	-336.15
0.1	0.4	-577.00	-387.70	-548.36	-335.51
0.1	0.5	-578.20	-388.23	-548.14	-311.05
0.2	0	-579.95	-386.79	-548.40	-337.40
0.2	0.1	-579.92	-386.86	-548.38	-337.34
0.2	0.2	-578.15	-386.58	-548.41	-336.96
0.2	0.3	-577.28	-386.21	-548.55	-336.33
0.2	0.4	-577.63	-386.32	-548.75	-335.81*
0.2	0.5	-578.83	-386.79	-548.90	-335.61
0.3	0	-578.94	-385.96	-547.96	-336.82
0.3	0.1	-579.99	-386.12	-547.70	-336.79
0.3	0.2	-579.07	-385.84	-547.70	-336.79
0.3	0.3	-578.14	-385.48	-547.97	-336.64
0.3	0.4	-578.73	-385.54	-548.48	-336.31
0.3	0.5	-579.95	-385.96	-548.98	-336.13
0.4	0	-578.20	-385.54	-548.03*	-336.39
0.4	0.1	-580.19	-385.73	-522.24	-336.37
0.4	0.2	-580.25	-385.44	-522.48	-336.68
0.4	0.3	-579.37	-385.10	-522.25	-336.90
0.4	0.4	-579.94	-385.15	-548.03	-336.87
0.4	0.5	-580.95	-385.54	-548.38	-336.63
0.5	0	-577.92	-385.39	-547.37*	-336.22
0.5	0.1	-580.24	-385.39	-547.92	-336.14
0.5	0.2	-580.75	-385.29	-548.08	-317.18
0.5	0.3	-579.98	-343.59	-548.08	-333.04
0.5	0.4	-580.55	-378.01	-547.92	-337.12
0.5	0.5	-581.29	-385.40	-547.37*	-336.89

Table S1: The tested total energies for the gamma-shift surface calculations conducted for each of the four model pure Fe GBs. “a-shift” and “b-shift” refer to the shift of the two grains with respect to one another in between the GB plane and the plane of atoms situated next to the GB plane. The shifts are in magnitudes given in fractional coordinates, corresponding to each cell dimensions used in the main text. * indicates non-converged calculations, but there are symmetrical equivalent structures that are converged that allow for us to draw the conclusions in the main text.

system	x ₀	y ₀	z ₀	x _{end}	y _{end}	z _{end}	E _{seg}
1	0.2750	0.0147	0.3659	0.1254	0.0064	0.3648	2.46
2	0.9750	0.1618	0.4341	0.9994	0.3247	0.4524	-1.08
3	0.1250	0.2206	0.4432	0.0168	0.3431	0.4539	-0.85
4	0.1250	0.4559	0.4432	0.0241	0.3485	0.4540	-0.85
5	0.2750	0.3088	0.4432	0.0295	0.3457	0.4540	-0.85
7	0.3750	0.9559	0.4432	0.4756	0.8484	0.4540	-0.85
8	0.3750	0.7206	0.4432	0.4824	0.8420	0.4540	-0.85
9	0.2250	0.7500	0.4523	0.4821	0.8443	0.4541	-0.85
10	0.3750	0.6324	0.3659	0.2342	0.7102	0.3643	2.10
11	0.2750	0.2500	0.4523	0.0174	0.3435	0.4540	-0.85
12	0.9750	0.5147	0.4523	0.9781	0.3502	0.4541	-0.85
13	0.0750	0.5441	0.4568	0.0383	0.3529	0.4543	-0.85
14	0.1250	0.7794	0.4568	0.4543	0.8474	0.4543	-0.85
15	0.2750	0.1912	0.4568	0.0104	0.3379	0.4540	-0.84
16	0.2250	0.6912	0.4568	0.4892	0.8370	0.4540	-0.84
17	0.3750	0.2794	0.4568	0.0489	0.3471	0.4544	-0.85
18	0.4250	0.0441	0.4568	0.4592	0.8531	0.4544	-0.85
21	0.2750	0.9265	0.3750	0.4993	0.8212	0.3975	-0.47
22	0.9750	0.8382	0.4705	0.0000	0.9012	0.4911	-0.12
24	0.2250	0.5735	0.4705	0.3225	0.5370	0.4914	-0.10
25	0.2250	0.4853	0.4795	0.3213	0.5352	0.4915	-0.10
26	0.3750	0.3677	0.4795	0.4981	0.4017	0.4912	-0.12
28	0.1250	0.1324	0.4795	0.1739	0.0388	0.4915	-0.10
29	0.1250	0.8677	0.4795	0.0020	0.9019	0.4912	-0.12
30	0.2750	0.9853	0.4795	0.1779	0.0352	0.4915	-0.10
31	0.2750	0.2500	0.5114	0.0045	0.3262	0.5094	-1.07
32	0.2750	0.8382	0.3841	0.4943	0.8165	0.3980	-0.47
33	0.2250	0.7500	0.5114	0.4955	0.8262	0.5094	-1.07
34	0.0250	0.5147	0.5114	0.0006	0.3303	0.5094	-1.07
35	0.3750	0.7206	0.3886	0.4920	0.8209	0.3976	-0.47
36	0.2250	0.7500	0.3932	0.4890	0.8174	0.3978	-0.47
37	0.3750	0.2794	0.4023	0.0755	0.3575	0.3977	-0.89
38	0.2750	0.1618	0.4068	0.0039	0.3048	0.3983	-0.47

Table S2: The tested interstitial P sites for the $\Sigma 3(1\bar{1}1)$ GB. The initial sites are denoted with subscript “0”, whereas their final relaxed coordinates are denoted with subscript “end”. Fractional coordinates are given such that they correspond to the POSCAR files in the beginning of the S.I.

system	x ₀	y ₀	z ₀	x _{end}	y _{end}	z _{end}	E _{seg}
1	0.8750	0.7708	0.3678	0.8282	0.8418	0.3602	1.50
2	0.8750	0.5625	0.4351	0.7650	0.4535	0.4377	1.49
3	0.3750	0.4375	0.4639	0.2833	0.4047	0.4665	1.06
4	0.9750	0.3542	0.3726	0.8260	0.4094	0.3556	1.32
5	0.6250	0.9375	0.4639	0.7191	0.9069	0.4668	1.05
6	0.1250	0.1042	0.4784	0.2074	0.1505	0.4949	1.06
7	0.8750	0.6042	0.4784	0.7890	0.6520	0.4952	1.05
8	0.2750	0.4375	0.4832	0.2111	0.6466	0.4950	1.06
9	0.7250	0.9375	0.4832	0.7883	0.1474	0.4951	1.06
10	0.0250	0.1458	0.4832	0.2099	0.1560	0.4955	1.05
11	0.1250	0.2292	0.4928	0.2094	0.1548	0.4954	1.05
12	0.8750	0.7292	0.4928	0.7906	0.6542	0.4954	1.06
13	0.2250	0.0208	0.3870	0.2474	0.8038	0.3799	1.50
14	0.2250	0.1875	0.5120	0.2873	0.3977	0.5047	1.05
15	0.3750	0.0208	0.5120	0.2896	0.9066	0.5046	1.05
16	0.4750	0.4375	0.5120	0.3027	0.4018	0.5237	1.05
17	0.7250	0.7292	0.4303	0.7469	0.8977	0.4418	1.12

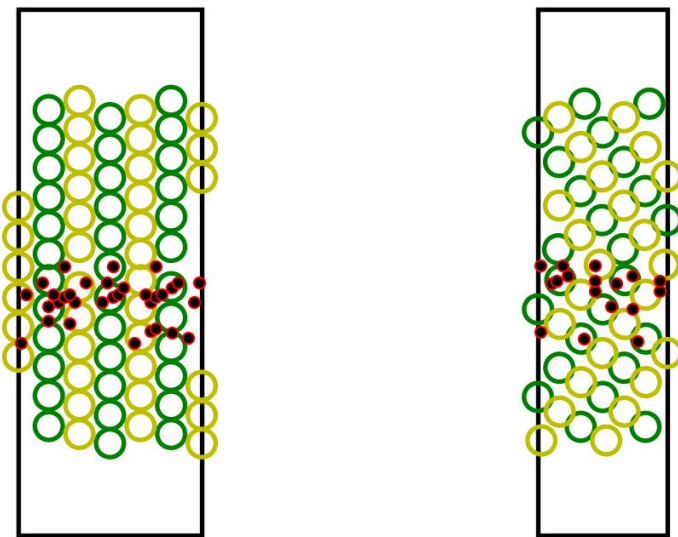
Table S3: The tested interstitial P sites for the $\Sigma 3(1\bar{1}2)$ GB. The initial sites are denoted with subscript “0”, whereas their final relaxed coordinates are denoted with subscript “end”. Fractional coordinates are given such that they correspond to the POSCAR files in the beginning of the S.I.

system	x ₀	y ₀	z ₀	x _{end}	y _{end}	z _{end}	E _{seg}
1	0.1774	0.3250	0.3799	0.2907	0.4815	0.3667	0.02
2	0.9194	0.8250	0.3799	0.8376	0.7319	0.3842	0.05
3	0.7581	0.6625	0.4508	0.6141	0.3245	0.4526	-1.35
4	0.2204	0.6250	0.4521	0.2547	0.6285	0.4690	-0.71
5	0.9839	0.7750	0.4534	0.9711	0.9818	0.4664	-0.79
6	0.9452	0.2250	0.4547	0.9654	0.9874	0.4664	-0.77
7	0.6936	0.9750	0.4547	0.6127	0.2866	0.4527	-1.36
8	0.4548	0.1950	0.4555	0.6094	0.2914	0.4527	-1.36
9	0.2312	0.3417	0.4679	0.9694	0.9851	0.4665	-0.77
10	0.2258	0.8500	0.4685	0.9724	0.9855	0.4666	-0.78
11	0.6505	0.8250	0.4731	0.6161	0.8082	0.4904	-1.35
12	0.9194	0.0750	0.3839	0.8384	0.1046	0.3843	0.04
13	0.8871	0.4250	0.4744	0.9602	0.4804	0.4768	-0.77
14	0.4839	1.0000	0.4803	0.6156	0.8110	0.4905	-1.35
15	0.4613	0.4950	0.4807	0.6150	0.8030	0.4905	-1.36
16	0.0968	0.1000	0.4862	0.9694	0.9861	0.4669	-0.78
17	0.3387	0.7750	0.4862	0.6128	0.8088	0.4906	-1.36
18	0.0806	0.9250	0.4902	0.9716	0.9650	0.4669	-0.78
19	0.8226	0.7750	0.5039	0.6062	0.8087	0.4908	-1.36
20	0.1452	0.4750	0.3917	0.9737	0.2968	0.3942	0.06
21	0.7903	0.8750	0.5138	0.6050	0.8097	0.4910	-1.36
22	0.9839	0.6250	0.5138	0.2464	0.6248	0.5166	-0.72
23	0.1129	0.5750	0.5138	0.2478	0.6246	0.5166	-0.72
24	0.9839	0.3750	0.5138	0.2442	0.6161	0.5165	-0.71
25	0.2419	0.8750	0.5138	0.2504	0.6289	0.5165	-0.71
26	0.2419	0.3250	0.5138	0.2510	0.6211	0.5166	-0.71

Table S4: The tested interstitial P sites for the $\Sigma 9(2\bar{2}1)$ GB. The initial sites are denoted with subscript “0”, whereas their final relaxed coordinates are denoted with subscript “end”. Fractional coordinates are given such that they correspond to the POSCAR files in the beginning of the S.I.

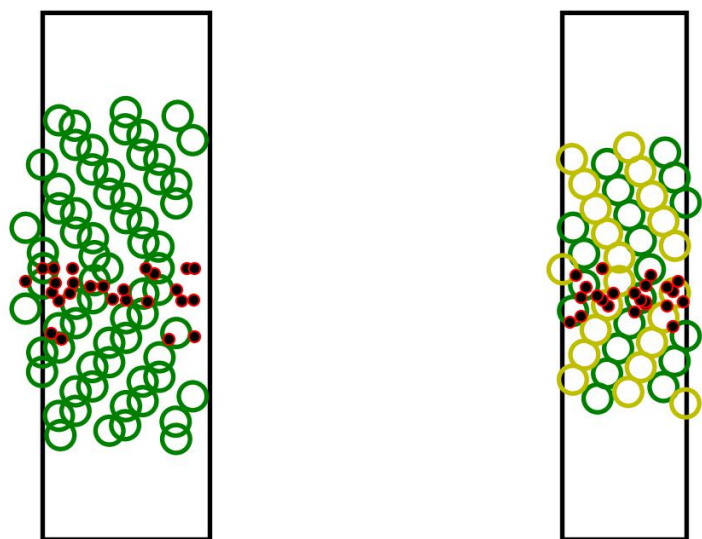
system	x ₀	y ₀	z ₀	x _{end}	y _{end}	z _{end}	E _{seg}
1	0.4750	0.3696	0.4429	0.2208	0.6305	0.4452	-1.04
2	0.1250	0.6739	0.4469	0.2161	0.6364	0.4452	-1.03
3	0.0750	0.6739	0.4508	0.2145	0.6352	0.4453	-1.03
4	0.2250	0.9783	0.4508	0.2340	0.1379	0.4691	-1.02
5	0.3750	0.3261	0.4547	0.4966	0.3104	0.4613	-0.81
6	0.9750	0.6304	0.4547	0.9867	0.7941	0.4528	-0.81
7	0.2250	0.1522	0.4587	0.2331	0.1415	0.4693	-1.02
8	0.2250	0.2826	0.4626	0.4915	0.3112	0.4646	-0.81
9	0.1250	0.5870	0.4665	0.4913	0.8063	0.4856	-0.78
10	0.2250	0.4130	0.4665	0.4972	0.3169	0.4648	-0.81
11	0.4750	0.8913	0.4705	0.4994	0.8141	0.4856	-0.78
12	0.3250	0.8478	0.4784	0.4962	0.8084	0.4890	-0.79
13	0.9750	0.1957	0.4784	0.9994	0.2819	0.4753	0.45
14	0.2250	0.6739	0.4823	0.4915	0.8051	0.4891	-0.79
15	0.2250	0.8913	0.4035	0.2067	0.1322	0.4204	-1.03
16	0.2250	0.9348	0.4902	0.4939	0.8124	0.4893	-0.79
17	0.9750	0.7174	0.5020	0.7527	0.6512	0.4941	-1.01
18	0.2750	0.1087	0.5020	0.4912	0.3007	0.5107	-0.78
19	0.2250	0.3261	0.5138	0.4934	0.3096	0.5138	-0.79
20	0.2750	0.0652	0.4114	0.1940	0.1345	0.4205	-1.06
21	0.1250	0.1522	0.4232	0.1915	0.1372	0.4208	-1.06
22	0.2250	0.5870	0.4311	0.2142	0.6371	0.4449	-1.04
23	0.2250	0.8478	0.4429	0.4934	0.8348	0.4406	-0.81

Table S5: The tested interstitial P sites for the $\Sigma 11(3\bar{3}2)$ GB. The initial sites are denoted with subscript “0”, whereas their final relaxed coordinates are denoted with subscript “end”. Fractional coordinates are given such that they correspond to the POSCAR files in the beginning of the S.I.



(a)

(b)



(c)

(d)

Figure S2: A visualisation of the tested interstitial positions in our study. The positions are plotted for the S2a $\Sigma_3(1\bar{1}1)$ S2b $\Sigma_3(1\bar{1}2)$ S2c $\Sigma_9(2\bar{2}1)$ S2d and $\Sigma_{11}(3\bar{3}2)$ GBs.

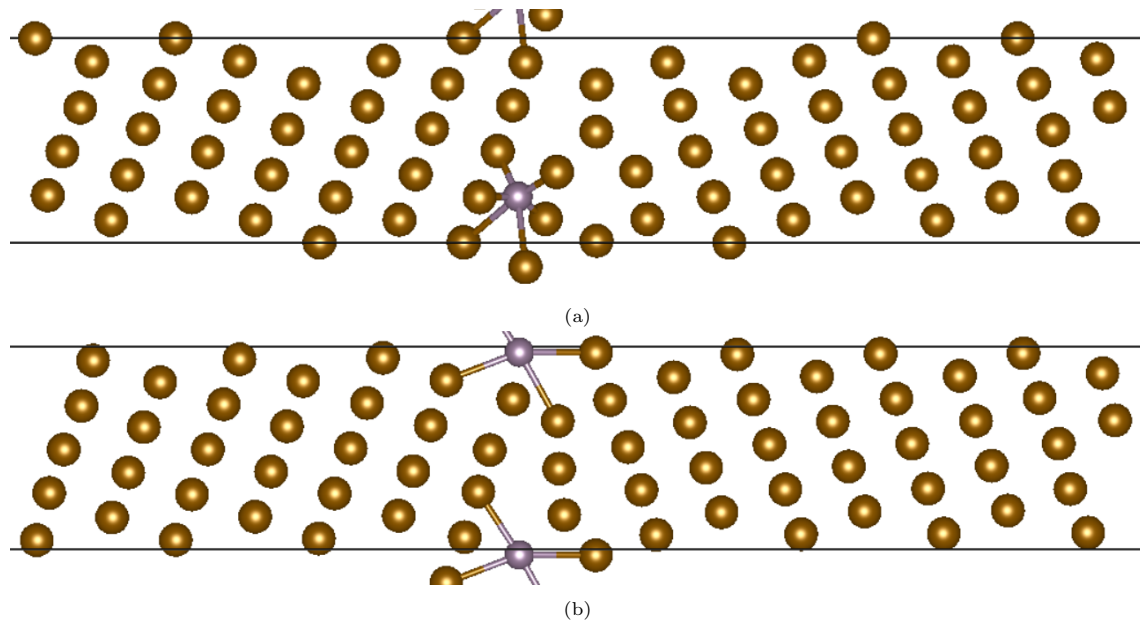


Figure S3: An example of the relaxation of an interstitial P site back into a substitutional site upon ionic optimisation in the $\Sigma 9(2\bar{2}1)$. This specific case is case 11 in Table S4. This “artefact” is present in all tested interstitial sites in the $\Sigma 9(2\bar{2}1)$ GB which yielded negative energies.

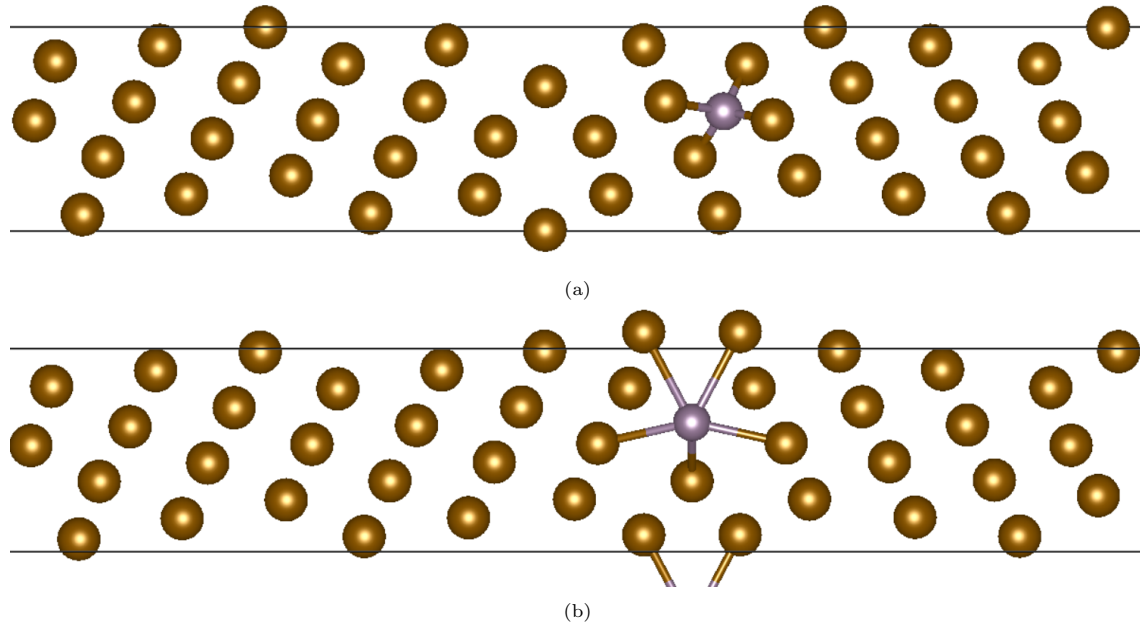


Figure S4: An example of the relaxation of an interstitial P site back into a substitutional site upon ionic optimisation in the $\Sigma 11(3\bar{3}2)$. This specific case is case 22 in Table S5. This “artefact” is present in all tested interstitial sites in the $\Sigma 11(3\bar{3}2)$ GB which yielded negative energies.

5.2. Substitutional segregation

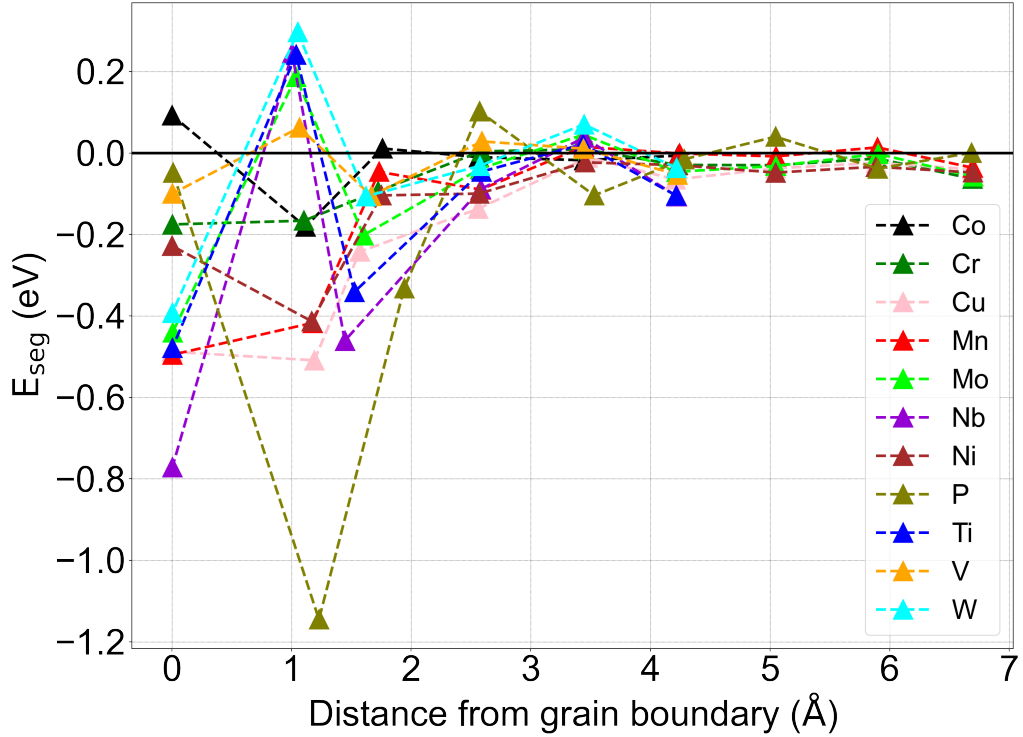


Figure S5: The segregation energy profiles of the tested substitutional solutes as a function of distance from the GB interface for the $\Sigma 3[110](1\bar{1}\bar{1})$ GBs.

site	distance (\AA)	multiplicity	Segregation energies (E_{seg}) (substitutional) (eV)											
			volume (\AA^3)	P	Ti	V	Cr	Mn	Co	Ni	Cu	Nb	Mo	W
20	6.7	4	11.38	0.00			-0.06	-0.04		-0.05	-0.04		-0.06	
22	5.9	4	11.38	-0.04			-0.01	0.01		-0.03	-0.02		0.00	
24	5.1	4	11.42	0.04			-0.03	-0.01		-0.05	-0.04		-0.03	
26	4.2	4	11.49	-0.02	-0.11	-0.05	-0.03	0.00	-0.01	-0.03	-0.07	-0.11	-0.05	-0.04
28	3.4	4	11.32	-0.10	0.02	0.01	0.01	0.02	-0.02	-0.02	-0.01	0.04	0.05	0.07
30	2.6	4	11.57	0.10	-0.05	0.03	0.00	-0.09	-0.01	-0.10	-0.14	-0.09	-0.04	-0.03
32	1.7	4	12.41	-0.33	-0.34	-0.11	-0.09	-0.05	0.01	-0.10	-0.24	-0.46	-0.20	-0.11
34	1.1	4	11.22	-1.15	0.24	0.06	-0.17	-0.42	-0.18	-0.41	-0.51	0.25	0.19	0.30
36	0.0	2	13.15	-0.05	-0.48	-0.10	-0.18	-0.50	0.09	-0.23	-0.49	-0.77	-0.44	-0.39

Table S6: The segregation energies of the substitutional solutes of P, Ti, V, Cr, Mn, Co, Ni, Cu, Nb, Mo and W are presented for the $\Sigma 3[110](1\bar{1}\bar{1})$. The Voronoi volume for the site in the pure GB is presented. Sites are available in the attached poscar files (0 indexed).

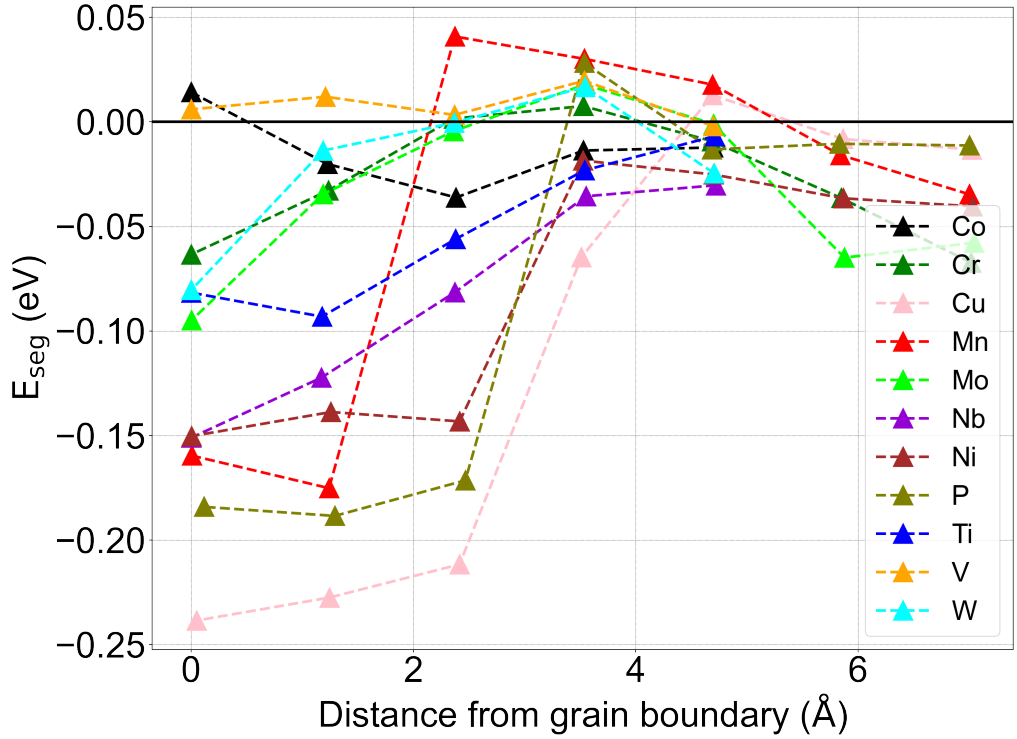


Figure S6: The segregation energy profiles of the tested substitutional solutes as a function of distance from the GB interface for the $\Sigma 3[110](\bar{1}\bar{1}2)$ GBs.

site	distance (Å)	multiplicity	Segregation energies (E_{seg}) (substitutional) (eV)											
			volume (\AA^3)	P	Ti	V	Cr	Mn	Co	Ni	Cu	Nb	Mo	W
12	7.0	4	11.32	-0.01			-0.07	-0.04		-0.04	-0.01		-0.06	
14	5.9	4	11.34	-0.01			-0.04	-0.02		-0.04	-0.01		-0.07	
16	4.7	4	11.36	-0.01	-0.01	0.00	-0.01	0.02	-0.01	-0.03	0.01	-0.03	0.00	-0.03
18	3.5	4	11.39	0.03	-0.02	0.02	0.01	0.03	-0.01	-0.02	-0.07	-0.04	0.02	0.02
20	2.4	4	11.45	-0.17	-0.06	0.00	0.00	0.04	-0.04	-0.14	-0.21	-0.08	0.00	0.00
22	1.2	4	11.64	-0.19	-0.09	0.01	-0.03	-0.18	-0.02	-0.14	-0.23	-0.12	-0.04	-0.01
24	0.0	2	11.83	-0.18	-0.08	0.01	-0.06	-0.16	0.01	-0.15	-0.24	-0.15	-0.10	-0.08

Table S7: The segregation energies of the substitutional solutes of Ti, V, Cr, Mn, Co, Ni, Cu, Nb, Mo and W are presented for the $\Sigma 3[110](\bar{1}\bar{1}2)$. The Voronoi volume for the site in the pure GB is presented. Sites are available in the attached poscar files (0 indexed).

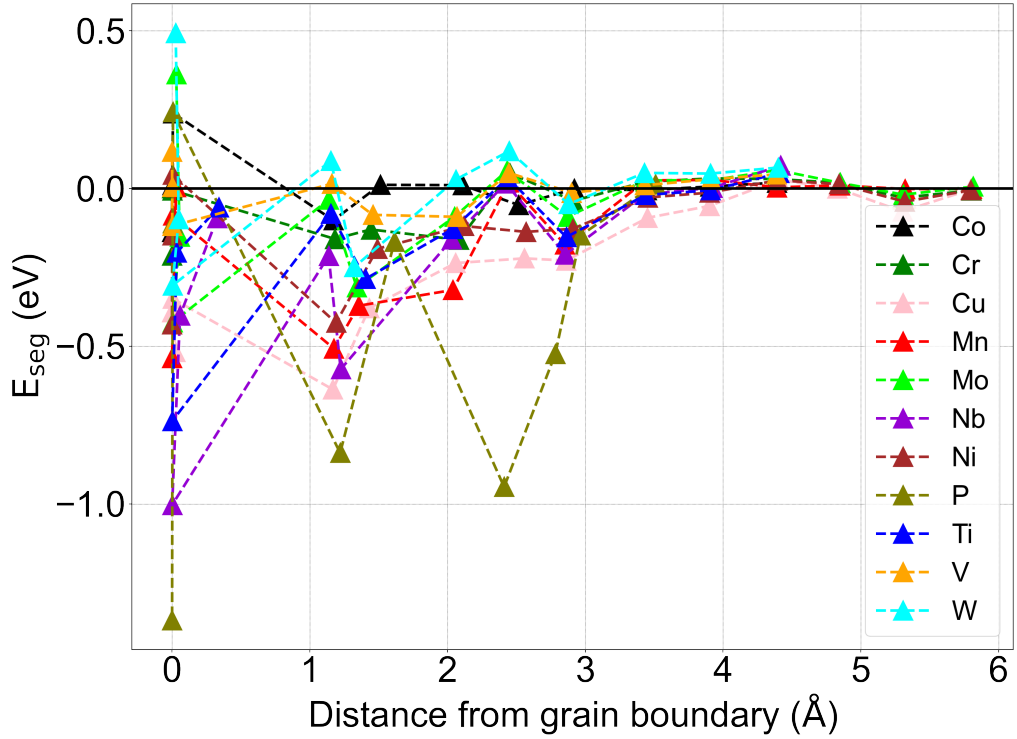


Figure S7: The segregation energy profiles of the tested substitutional solutes as a function of distance from the GB interface for the $\Sigma 9[110](\bar{2}\bar{2}1)$ GB.

site	distance (Å)	no.	volume (\AA^3)	Segregation energies (E_{seg}) (substitutional) (eV)												
				P	P-old	Ti	V	Cr	Mn	Co	Ni	Cu	Nb	Mo	W	
23	5.8	2	11.37		0.02			-0.01	0.00		-0.01	0.00		0.01		
24	5.3	2	11.43		0.05			-0.03	0.00		-0.04	-0.07		-0.02		
25	4.8	2	11.41		0.04			0.02	0.01		0.01	0.00		0.02		
26	4.4	2	11.30		0.03	0.05	0.05	0.03	0.00	0.02	0.03	0.03	0.07	0.06	0.07	
27	3.9	2	11.44		0.08	-0.01	0.03	0.03	0.03	0.03	0.01	-0.01	-0.06	0.00	0.03	0.05
28	3.4	2	11.38	0.01	0.03	-0.02	0.01	0.02	0.03	-0.01	-0.03	-0.09	-0.02	0.03	0.05	
29	2.9	2	11.89	-0.15	-0.07	-0.15	-0.01	-0.04	-0.18	0.00	-0.13	-0.23	-0.21	-0.09	-0.05	
30	2.5	2	11.55	-0.53	-0.64	0.03	0.05	0.05	0.02	-0.05	-0.14	-0.22	0.02	0.06	0.12	
31	2.1	2	11.56	-0.95	-1.34	-0.13	-0.09	-0.16	-0.32	0.01	-0.12	-0.24	-0.16	-0.09	0.03	
32	1.5	2	12.14	-0.17	0.02	-0.29	-0.08	-0.13	-0.37	0.01	-0.19	-0.38	-0.57	-0.31	-0.25	
33	1.2	2	11.43	-0.84	-0.81	-0.08	0.02	-0.16	-0.51	-0.10	-0.43	-0.64	-0.21	-0.04	0.09	
34	0	1	13.86	0.24	0.00	-0.74	-0.12	-0.01	-0.09	0.24	0.04	-0.35	-1.00	-0.43	-0.31	
35	0	1	12.11	-0.11	-0.09	-0.20	0.01	0.00	0.00	0.01	-0.15	-0.39	-0.40	-0.15	-0.10	
36	0	1	10.66	-1.37	-1.36	-0.06	0.12	-0.21	-0.54	-0.14	-0.43	-0.52	-0.09	0.36	0.49	

Table S8: The segregation energies of the substitutional solutes of Ti, V, Cr, Mn, Co, Ni, Cu, Nb, Mo and W are presented for the $\Sigma 9[110](\bar{2}\bar{2}1)$. “P” is calculated using a 2×1 cell (compared to the dimensions given in the main text). “P-old” is the profile calculated using the original cell. The Voronoi volume for the site in the pure GB is presented. Sites are available in the attached poscar files (0 indexed).

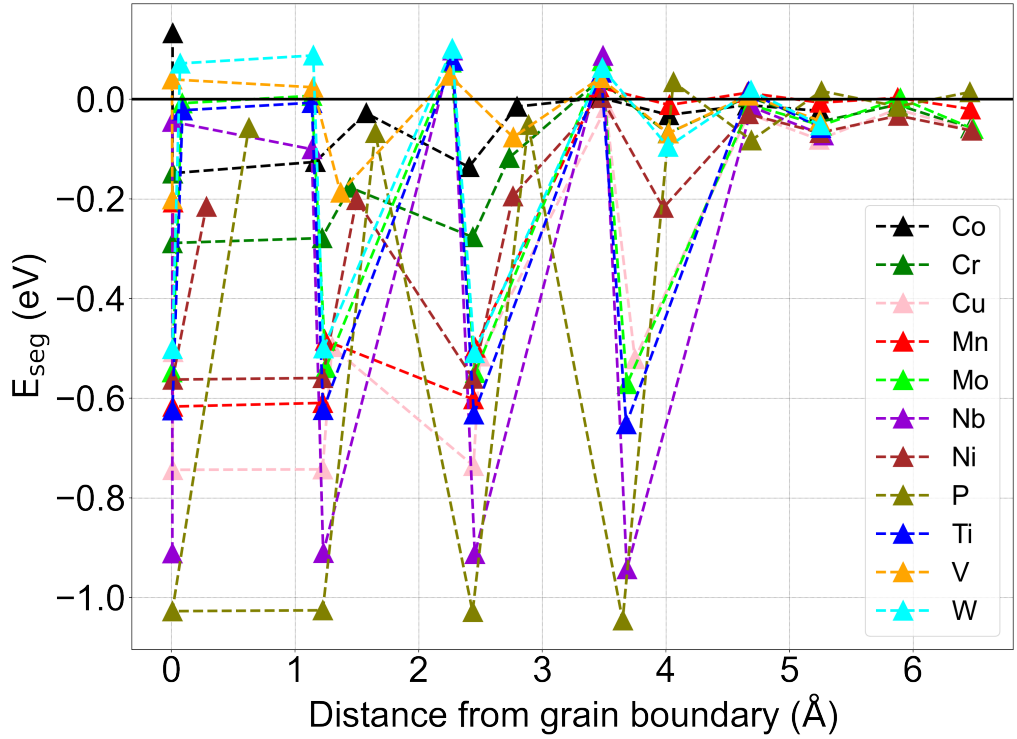


Figure S8: The segregation energy profiles of the tested substitutional solutes as a function of distance from the GB interface for the $\Sigma 11[110](\bar{3}\bar{3}2)$ GBs. The peculiarity of the similar energies across the same sites for certain solutes in the $\Sigma 11[110](\bar{3}\bar{3}2)$ GB is due to local interface reconstruction via relaxation. This is observed in Figs. S4 and S10. Sites are available in the attached poscar files (0 indexed). In the subsequent Fig. S9, the segregation profiles calculated in a 2×2 cell is presented.

site	distance (Å)	# sites	volume (\AA^3)	Segregation energies (E_{seg}) (substitutional) (eV)										
				P	Ti	V	Cr	Mn	Co	Ni	Cu	Nb	Mo	W
11	6.5	2	11.39	0.01			-0.06	-0.02		-0.06	-0.06		-0.06	
12	5.9	2	11.34	-0.01			-0.01	0.00		-0.03	-0.02		0.00	
13	5.2	2	11.43	0.02	-0.06	-0.04	-0.05	-0.01	-0.02	-0.07	-0.08	-0.07	-0.05	-0.05
14	4.7	2	11.33	-0.08	0.02	0.01	0.01	0.01	-0.01	-0.03	-0.03	-0.02	-0.01	0.02
15	4.0	2	11.49	0.04	-0.65	-0.07	-0.07	-0.01	-0.03	-0.22	-0.52	-0.94	-0.57	-0.10
16	3.5	2	11.27	-1.05	0.05	0.04	0.04	0.02	0.00	0.00	-0.02	0.09	0.08	0.06
17	2.8	2	11.8	-0.05	-0.63	-0.08	-0.12	-0.50	-0.02	-0.20	-0.52	-0.91	-0.55	-0.51
18	2.3	2	11.24	-1.03	0.08	0.05	-0.28	-0.60	-0.14	-0.56	-0.74	0.10	0.07	0.10
19	1.5	2	12.39	-0.07	-0.62	-0.19	-0.18	-0.48	-0.03	-0.20	-0.50	-0.91	-0.54	-0.50
20	1.2	2	11.27	-1.03	-0.01	0.02	-0.28	-0.61	-0.13	-0.56	-0.74	-0.10	0.01	0.09
21	0.0	1	11.31	-1.03	-0.02	0.04	-0.29	-0.62	-0.15	-0.56	-0.74	-0.05	-0.01	0.07
22	0.0	1	13.05	-0.06	-0.62	-0.20	-0.15	-0.21	0.13	-0.22	-0.51	-0.91	-0.55	-0.50

Table S9: The segregation energies of the substitutional solutes of P, Ti, V, Cr, Mn, Co, Ni, Cu, Nb, Mo and W are presented for the $\Sigma 11[110](\bar{3}\bar{3}2)$. The Voronoi volume for the site in the pure GB is presented. Sites are available in the attached poscar files (0 indexed).

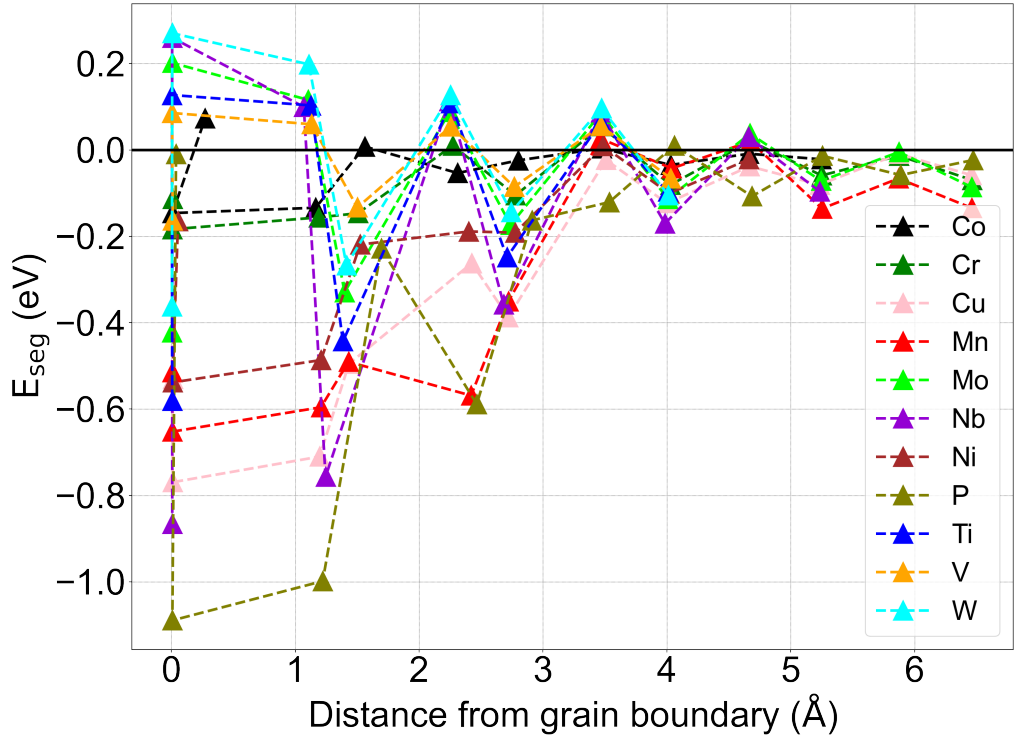


Figure S9: The segregation energy profiles of the tested substitutional solutes as a function of distance from the GB interface for the $\Sigma 11[110](\bar{3}\bar{3}2)$ GBs. The results in this Table are those presented in the main text. These results were also used to calculate the subsequent E_{int} values in the co-segregation cases.

Segregation energies (substitutional) (eV)														
site	distance (Å)	# sites	volume (\AA^3)	P	Ti	V	Cr	Mn	Co	Ni	Cu	Nb	Mo	W
11	6.5	4	11.39	-0.02			-0.07	-0.14			-0.06		-0.09	
12	5.9	4	11.34	-0.06			-0.01	-0.07			-0.01		-0.01	
13	5.2	4	11.43	-0.01			-0.06	-0.14	-0.02		-0.08	-0.10	-0.07	
14	4.7	4	11.33	-0.11			0.02	0.02	-0.01	-0.02	-0.04	0.03	0.04	
15	4.0	4	11.49	0.01	-0.10	-0.07	-0.08	-0.04	-0.04	-0.10	-0.12	-0.17	-0.11	
16	3.5	4	11.27	-0.12	0.06	0.06	0.06	0.03	0.00	0.01	-0.02	0.09	0.09	
17	2.8	4	11.8	-0.16	-0.25	-0.09	-0.11	-0.35	-0.02	-0.19	-0.39	-0.36	-0.17	
18	2.3	4	11.24	-0.59	0.11	0.05	0.01	-0.57	-0.05	-0.19	-0.26	0.11	0.09	
19	1.5	4	12.39	-0.23	-0.44	-0.13	-0.15	-0.49	0.01	-0.22	-0.50	-0.76	-0.33	
20	1.2	4	11.27	-1.00	0.10	0.06	-0.16	-0.60	-0.13	-0.49	-0.71	0.10	0.12	
21	0.0	2	11.31	-1.09	0.13	0.09	-0.18	-0.65	-0.15	-0.54	-0.77	0.26	0.20	
22	0.0	2	13.05	-0.01	-0.58	-0.16	-0.11	-0.52	0.07	-0.17	-0.53	-0.87	-0.42	

Table S10: The segregation energies of the substitutional solutes of P, Ti, V, Cr, Mn, Co, Ni, Cu, Nb, Mo and W are presented for the $\Sigma 11[110](\bar{3}\bar{3}2)$. The Voronoi volume for the site in the pure GB is presented.

5.3. Interfacial reconstruction phenomena

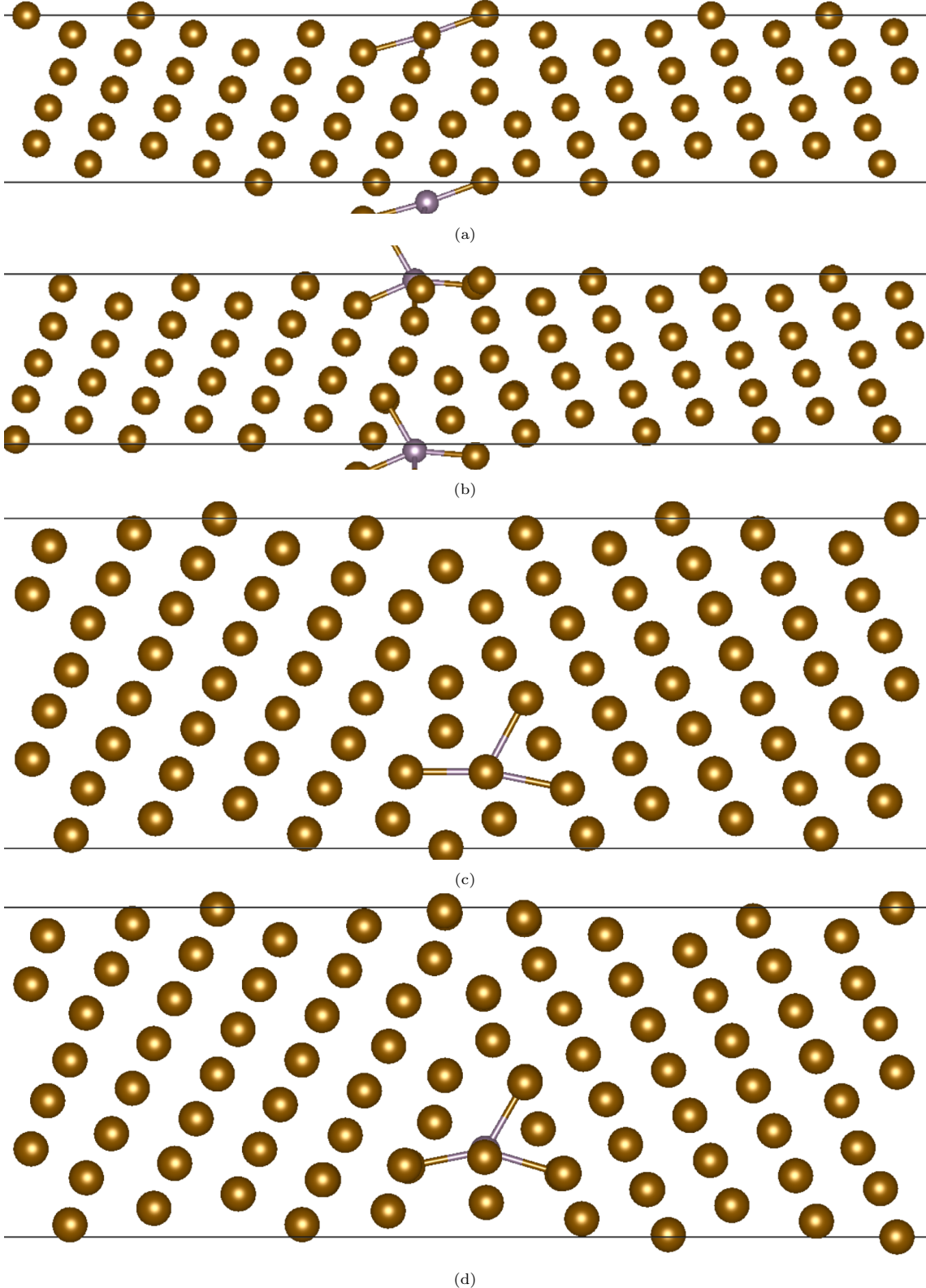


Figure S10: The interfacial reconstruction phenomena are demonstrated in the larger cells ($2 \times 1 \Sigma 9(2\bar{2}1)$, $2 \times 2 \Sigma 11(3\bar{3}2)$). The reconstruction is visualised in the larger $\Sigma 9(2\bar{2}1)$ GB, for the S10a initial structure and S10b the final relaxed structure. The reconstruction is visualised in the larger $\Sigma 11(3\bar{3}2)$ GB, for the S10c initial structure and S10d the final relaxed structure. Notice the shift of the interface towards the segregated solute (in this case P). In this case, these particular polyhedral formations are not as rigid, and more vulnerable to warping due to segregation phenomena.

5.4. Cleavage planes tested

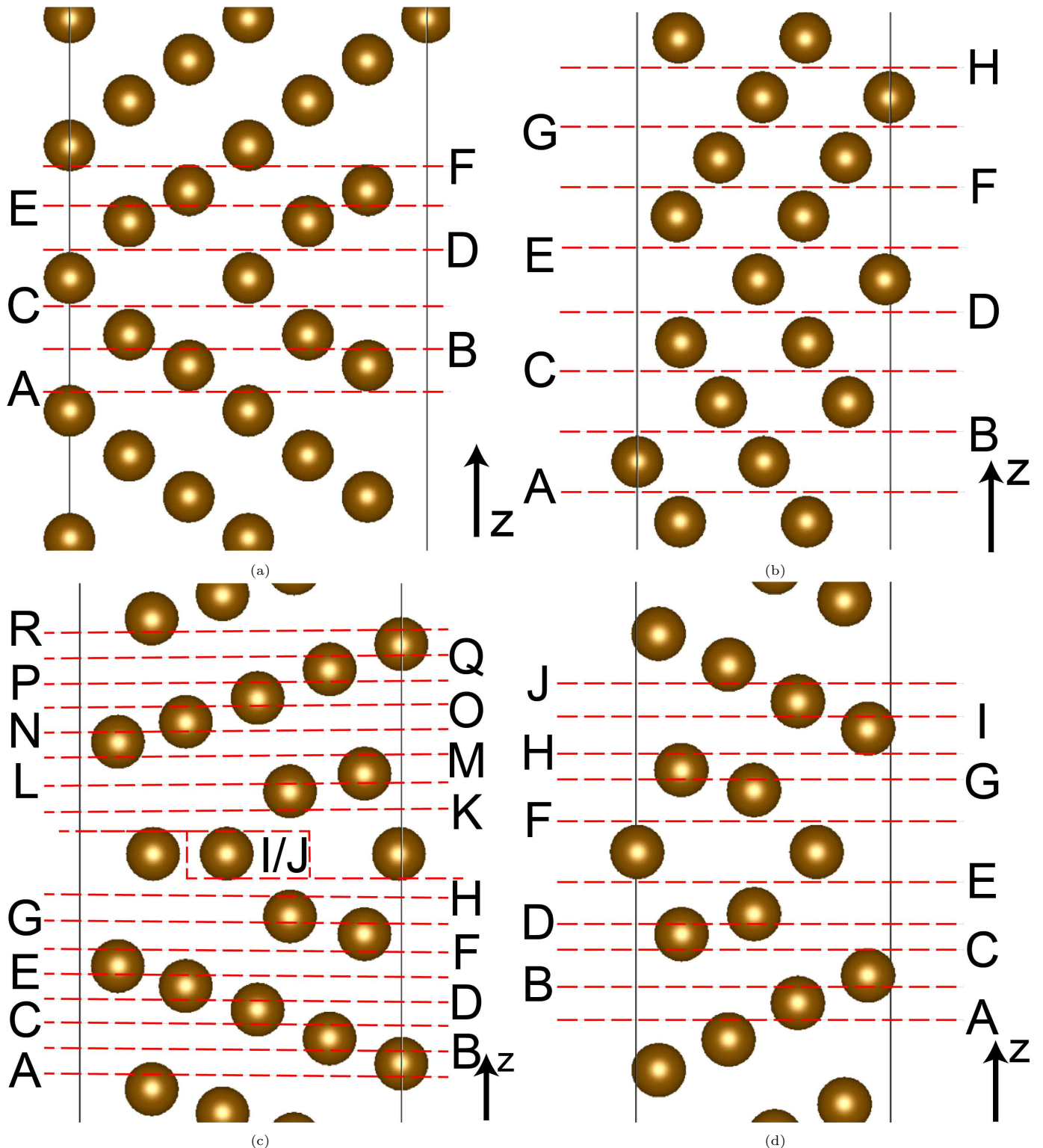


Figure S11: The cleavage planes tested for the S11a $\Sigma 3[110](1\bar{1}1)$ S11b $\Sigma 3[110](1\bar{1}2)$ S11c $\Sigma 9[110](2\bar{2}1)$ S11d $\Sigma 11[110](3\bar{3}2)$ GBs. The positive directions of the cleavage planes are indicated. Sites are indexed from 0-n along the axis indicated, increasing in index as we move towards the positive direction.

system	E_{seg} (eV)	$W_{\text{sep}}^{\text{RGS}}$ (J/m ²)	η_{RGS} (J/m ²)	CP_{RGS}	$W_{\text{sep}}^{\text{rel}}$ (J/m ²)	η_{rel} (J/m ²)	ANSBO (BO/Å ²)	η_{ANSBO} (BO/Å ²)	CP_{ANSBO}	SBO(N)	$\Delta \text{SBO}(N)$
Co-34-d-1.1	-0.18	4.18	-0.02	0.520	3.78	-0.02	0.156	-0.002	0.505	4.07	-0.17
Cr-34-d-1.1	-0.17	4.18	-0.02	0.505	3.87	0.07	0.159	0.001	0.505	4.11	-0.13
Cr-36-d-0.0	-0.18	4.27	0.07	0.520	3.88	0.07	0.155	-0.004	0.520	3.36	-0.13
Cu-34-d-1.1	-0.51	3.97	-0.24	0.505	3.53	-0.27	0.146	-0.012	0.505	3.51	-0.73
Cu-36-d-0.0	-0.49	3.94	-0.26	0.520	3.52	-0.28	0.148	-0.010	0.505	2.88	-0.61
Mn-36-d-0.0	-0.50	4.33	0.13	0.520	4.03	0.23	0.154	-0.004	0.520	3.53	0.05
Mo-36-d-0.0	-0.44	4.68	0.48	0.520	4.14	0.33	0.163	0.005	0.520	4.67	1.18
Nb-36-d-0.0	-0.77	4.41	0.21	0.520	3.98	0.18	0.157	-0.001	0.520	4.48	0.99
Ni-34-d-1.1	-0.41	4.13	-0.07	0.505	3.78	-0.03	0.150	-0.008	0.505	3.86	-0.38
P-34-d-1.1	-1.15	3.85	-0.35	0.505	3.60	-0.21	0.162	0.004	0.505	4.83	0.60
Ti-36-d-0.0	-0.48	4.19	-0.01	0.520	3.84	0.03	0.154	-0.004	0.520	3.27	-0.22
V-32-d-1.7	-0.11	4.33	0.13	0.520	3.93	0.12	0.159	0.001	0.505	3.72	-0.05
V-36-d-0.0	-0.10	4.35	0.15	0.520	3.91	0.10	0.156	-0.002	0.520	3.46	-0.03
W-36-d-0.0	-0.39	5.01	0.81	0.520	4.36	0.56	0.169	0.011	0.520	5.18	1.69
GB		4.20		3.81		0.158					

Table S11: The associated data with the 1-solute segregation case for the $\Sigma 3(1\bar{1}1)$. The segregation energy (E_{seg}), rigid work of separation ($W_{\text{sep}}^{\text{RGS}}$), rigid cohesion change (η_{RGS}), fractional coordinates (z) of the cleavage plane with minimum rigid work of separation (CP_{RGS}), relaxed work of separation ($W_{\text{sep}}^{\text{rel}}$), relaxed cohesion change (η_{rel}) area-normalised summed bond order at the weakest cleavage plane (ANSBO), ANSBO cohesion change (η_{ANSBO}), fractional coordinates (z) of the weakest cleavage plane as quantified by the ANSBO (CP_{ANSBO}) summed bond order of the solute atom (SBO(N)), and the change in the summed bond order compared to the Fe atom that it replaced ($\Delta \text{SBO}(N)$).

system	E_{seg} (eV)	$W_{\text{sep}}^{\text{RGS}}$ (J/m ²)	η_{RGS} (J/m ²)	CP_{RGS}	$W_{\text{sep}}^{\text{rel}}$ (J/m ²)	η_{rel} (J/m ²)	ANSBO (BO/Å ²)	η_{ANSBO} (BO/Å ²)	CP_{ANSBO}	SBO(N)	$\Delta \text{SBO}(N)$
Co-20-d-2.4	-0.04	4.93	0.05	0.53	4.75	0.03	0.155	0.000	0.53	3.79	-0.17
Co-22-d-1.2	-0.02	4.95	0.07	0.50	4.72	0.00	0.153	-0.001	0.50	3.78	-0.12
Cr-24-d-0.0	-0.06	5.01	0.13	0.53	4.81	0.09	0.155	0.001	0.53	3.70	-0.14
Cu-20-d-2.4	-0.21	4.43	-0.46	0.47	4.22	-0.50	0.149	-0.005	0.44	3.23	-0.73
Cu-22-d-1.2	-0.23	4.47	-0.41	0.50	4.25	-0.47	0.152	-0.002	0.50	3.22	-0.67
Cu-24-d-0.0	-0.24	4.43	-0.45	0.53	4.24	-0.48	0.147	-0.007	0.53	3.20	-0.64
Mn-22-d-1.2	-0.18	5.09	0.21	0.50	4.89	0.17	0.159	0.004	0.53	3.95	0.05
Mn-24-d-0.0	-0.16	4.96	0.08	0.53	4.85	0.13	0.159	0.005	0.53	3.91	0.07
Mo-24-d-0.0	-0.10	5.28	0.40	0.41	5.12	0.40	0.165	0.010	0.53	5.08	1.24
Nb-24-d-0.0	-0.15	4.98	0.10	0.53	4.67	-0.05	0.155	0.000	0.53	4.86	1.02
Ni-20-d-2.4	-0.14	4.69	-0.19	0.47	4.46	-0.27	0.152	-0.002	0.47	3.54	-0.41
Ni-22-d-1.2	-0.14	4.71	-0.17	0.50	4.48	-0.24	0.151	-0.004	0.50	3.55	-0.35
Ni-24-d-0.0	-0.15	4.69	-0.19	0.53	4.47	-0.26	0.147	-0.007	0.53	3.50	-0.34
P-20-d-2.4	-0.17	3.86	-1.02	0.47	3.65	-1.07	0.159	0.005	0.53	4.46	0.51
P-22-d-1.2	-0.19	3.92	-0.96	0.50	3.66	-1.06	0.159	0.005	0.53	4.42	0.52
P-24-d-0.0	-0.18	3.93	-0.95	0.50	3.66	-1.06	0.159	0.005	0.44	4.41	0.57
Ti-22-d-1.2	-0.09	4.98	0.10	0.47	4.67	-0.06	0.155	0.000	0.50	3.53	-0.36
Ti-24-d-0.0	-0.08	4.87	-0.01	0.53	4.66	-0.06	0.147	-0.007	0.53	3.52	-0.32
V-24-d-0.0	0.01	5.14	0.26	0.53	4.91	0.19	0.155	0.000	0.53	3.75	-0.09
W-24-d-0.0	-0.08	5.29	0.41	0.41	5.13	0.41	0.164	0.010	0.44	5.61	1.77
GB		4.88		4.72		0.15					

Table S12: The associated data with the 1-solute segregation case for the $\Sigma 3(1\bar{1}2)$. See above for abbreviation explanations.

system	E_{seg} (eV)	$W_{\text{sep}}^{\text{RGS}}$ (J/m ²)	η_{RGS} (J/m ²)	CP_{RGS}	$W_{\text{sep}}^{\text{rel}}$ (J/m ²)	η_{rel} (J/m ²)	ANSBO (BO/Å ²)	η_{ANSBO} (BO/Å ²)	CP_{ANSBO}	SBO(N)	$\Delta \text{SBO(N)}$
Co-33-d-1.2	-0.10	4.15	-0.04	0.52	3.60	0.00	0.139	-0.002	0.52	3.97	-0.13
Co-36-d-0.0	-0.14	4.29	0.09	0.50	3.72	0.12	0.140	-0.001	0.52	4.19	-0.19
Cr-36-d-0.0	-0.21	4.41	0.21	0.52	3.84	0.24	0.143	0.002	0.52	4.22	-0.16
Cu-33-d-1.2	-0.64	3.75	-0.45	0.50	3.40	-0.20	0.120	-0.022	0.48	3.26	-0.84
Mn-33-d-1.2	-0.51	4.33	0.14	0.50	3.86	0.26	0.133	-0.008	0.48	4.08	-0.02
Mn-36-d-0.0	-0.54	4.64	0.44	0.50	3.88	0.28	0.142	0.001	0.55	4.55	0.17
Mo-34-d-0.0	-0.43	4.78	0.59	0.50	4.00	0.40	0.148	0.006	0.48	4.50	1.21
Nb-34-d-0.0	-1.00	4.59	0.39	0.50	4.04	0.44	0.148	0.007	0.48	4.35	1.06
Ni-33-d-1.2	-0.43	4.03	-0.16	0.50	3.64	0.04	0.122	-0.019	0.50	3.66	-0.44
Ni-36-d-0.0	-0.43	4.23	0.04	0.50	3.65	0.05	0.138	-0.003	0.52	3.96	-0.42
P-36-d-0.0	-1.37	4.16	-0.03	0.52	3.57	-0.03	0.141	0.000	0.55	5.01	0.63
Ti-34-d-0.0	-0.74	4.41	0.21	0.50	3.90	0.30	0.144	0.003	0.50	3.13	-0.16
V-31-d-2.1	-0.09	4.16	-0.04	0.50	3.76	0.16	0.137	-0.005	0.50	3.93	-0.09
V-32-d-1.5	-0.08	4.34	0.14	0.50	3.87	0.27	0.137	-0.004	0.50	3.67	-0.09
V-34-d-0.0	-0.12	4.49	0.30	0.50	3.78	0.18	0.144	0.003	0.55	3.30	0.01
W-34-d-0.0	-0.31	4.97	0.77	0.48	3.90	0.30	0.149	0.008	0.48	5.00	1.71
GB		4.20			3.60		0.14				

Table S13: The associated data with the 1-solute segregation case for the $\Sigma 9(2\bar{2}1)$. The segregation energy (E_{seg}), rigid work of separation ($W_{\text{sep}}^{\text{RGS}}$), rigid cohesion change (η_{RGS}), fractional coordinates (z) of the cleavage plane with minimum rigid work of separation (CP_{RGS}), relaxed work of separation ($W_{\text{sep}}^{\text{rel}}$), relaxed cohesion change (η_{rel}) area-normalised summed bond order at the weakest cleavage plane (ANSBO), ANSBO cohesion change (η_{ANSBO}), fractional coordinates (z) of the weakest cleavage plane as quantified by the ANSBO (CP_{ANSBO}) summed bond order of the solute atom (SBO(N)), and the change in the summed bond order compared to the Fe atom that it replaced ($\Delta \text{SBO(N)}$).

system	E_{seg} (eV)	$W_{\text{sep}}^{\text{RGS}}$ (J/m ²)	η_{RGS} (J/m ²)	CP_{RGS}	$W_{\text{sep}}^{\text{rel}}$ (J/m ²)	η_{rel} (J/m ²)	ANSBO (BO/Å ²)	η_{ANSBO} (BO/Å ²)	CP_{ANSBO}	SBO(N)	$\Delta \text{SBO(N)}$
Co-21-d-0.0	-0.15	4.43	0.16	0.520	3.99	0.16	0.152	-0.002	0.520	3.98	-0.13
Cr-21-d-0.0	-0.18	4.61	0.34	0.520	4.17	0.34	0.154	0.000	0.495	3.94	-0.17
Cu-21-d-0.0	-0.77	4.07	-0.21	0.520	3.67	-0.16	0.145	-0.009	0.520	3.34	-0.77
Mn-21-d-0.0	-0.65	4.88	0.61	0.520	4.24	0.41	0.156	0.003	0.520	4.19	0.08
Mo-19-d-1.5	-0.33	5.06	0.78	0.496	4.51	0.68	0.162	0.008	0.496	4.70	1.02
Nb-22-d-0.0	-0.87	4.76	0.48	0.496	4.41	0.57	0.162	0.009	0.496	4.46	0.99
Ni-21-d-0.0	-0.54	4.38	0.10	0.520	4.00	0.17	0.149	-0.005	0.495	3.75	-0.37
P-21-d-0.0	-1.09	3.91	-0.37	0.520	3.45	-0.38	0.164	0.010	0.473	4.75	0.64
Ti-22-d-0.0	-0.58	4.53	0.25	0.496	4.19	0.36	0.153	0.000	0.496	3.21	-0.26
V-22-d-0.0	-0.16	4.72	0.45	0.496	4.18	0.35	0.156	0.002	0.496	3.46	-0.01
W-22-d-0.0	-0.36	5.30	1.03	0.473	4.40	0.56	0.167	0.014	0.473	5.22	1.76
GB		4.28			3.83		0.154				

Table S14: The associated data with the 1-solute segregation case for the $\Sigma 11(3\bar{3}2)$. The segregation energy (E_{seg}), rigid work of separation ($W_{\text{sep}}^{\text{RGS}}$), rigid cohesion change (η_{RGS}), fractional coordinates (z) of the cleavage plane with minimum rigid work of separation (CP_{RGS}), relaxed work of separation ($W_{\text{sep}}^{\text{rel}}$), relaxed cohesion change (η_{rel}) area-normalised summed bond order at the weakest cleavage plane (ANSBO), ANSBO cohesion change (η_{ANSBO}), fractional coordinates (z) of the weakest cleavage plane as quantified by the ANSBO (CP_{ANSBO}) summed bond order of the solute atom (SBO(N)), and the change in the summed bond order compared to the Fe atom that it replaced ($\Delta \text{SBO(N)}$).

6. Co-segregation energetics tables

solute 1	solute 2	$\Sigma 3(1\bar{1}1)$		$\Sigma 3(1\bar{1}2)$		$\Sigma 9(2\bar{2}1)$		$\Sigma 11(3\bar{3}2)$	
		E_{seg}^{inc} (eV)	E_{int} (eV)	E_{seg}^{inc} (eV)	E_{int} (eV)	E_{seg}^{inc} (eV)	E_{int} (eV)	E_{seg}^{inc} (eV)	E_{int} (eV)
P	Co	-0.12	0.06	-0.03	-0.01	-0.09	0.01	-0.03	0.1
P	Cr	-0.08	0.1	-0.01	0.02	-0.05	0.11	0.16	0.24
P	Cu	-0.58	-0.44	-0.31	-0.08	-0.51	0.13	-0.38	0.33
P	Mn	-0.47	0.03	-0.29	-0.12	-0.36	0.15	-0.19	0.41
P	Mo	-0.17	0.27	0.03	0.04	-0.14	0.28	-0.12	0.3
P	Nb	-0.53	0.24	-0.13	-0.01	-0.83	0.18	-0.52	0.34
P	Ni	-0.39	0.02	-0.2	-0.06	-0.37	0.05	-0.25	0.24
P	Ti	-0.46	0.02	-0.16	-0.08	-0.7	0.04	-0.32	0.26
P	V	-0.02	0.08	0.02	0.02	0.04	0.06	0.07	0.14
P	W	-0.04	0.35	0.03	0.01	-0.03	0.28	0.14	0.24

Table S15: The *minimum* incremental segregation energies (E_{seg}^{inc}) for “X” solute in P-X sequenced co-segregation pairings, and the corresponding interaction energies (E_{int}) that occur between the pairs at that specific configuration. In effect, this represents the situation where P is already segregated to the GB, with X attempting to co-segregate. Positive E_{int} values indicate repulsive interactions, and negative values indicate attraction. Positive E_{seg}^{inc} values exist because we only sampled sites with distances of <3.5 Å away from the interface.

solute 1	solute 2	$\Sigma 3(1\bar{1}1)$		$\Sigma 3(1\bar{1}2)$		$\Sigma 9(2\bar{2}1)$		$\Sigma 11(3\bar{3}2)$	
		E_{seg}^{inc} (eV)	E_{int} (eV)	E_{seg}^{inc} (eV)	E_{int} (eV)	E_{seg}^{inc} (eV)	E_{int} (eV)	E_{seg}^{inc} (eV)	E_{int} (eV)
Co	P	-1.08	0.06	-0.19	0	-1.21	-0.26	-0.92	0.08
Cr	P	-1.05	0.1	-0.1	0.07	-1.01	-0.06	-0.69	0.31
Cu	P	-1.19	-0.05	-0.26	-0.07	-1.28	0.09	-0.66	0.34
Mn	P	-1.12	0.03	-0.31	-0.12	-0.95	0	-0.63	0.37
Mo	P	-0.88	0.27	-0.04	0.13	-1.12	0.25	-0.72	0.27
Nb	P	-0.91	0.24	-0.12	0.05	-1.22	0.15	-0.66	0.43
Ni	P	-1.12	0.02	-0.23	-0.04	-1.06	-0.12	-0.69	0.31
P	P	-1.07	0.07	-0.25	-0.28	-0.69	0.15	-0.2	-0.08
Ti	P	-1.13	0.02	-0.25	-0.06	-1.36	0.01	-0.77	0.32
W	P	-0.79	0.35	0.01	-0.02	-1.12	0.25	-0.49	0.6

Table S16: The *minimum* incremental segregation energies (E_{seg}^{inc}) for P in X-P sequenced pairings calculated for co-segregation, and the corresponding interaction energies (E_{int}) that occur between the pairs at that specific configuration. In effect, this represents the situation where X is already segregated to the GB, with P attempting to co-segregate. Positive E_{int} values indicate repulsive interactions, and negative values indicate attraction.

7. Co-segregation interaction energy (E_{int}) plots

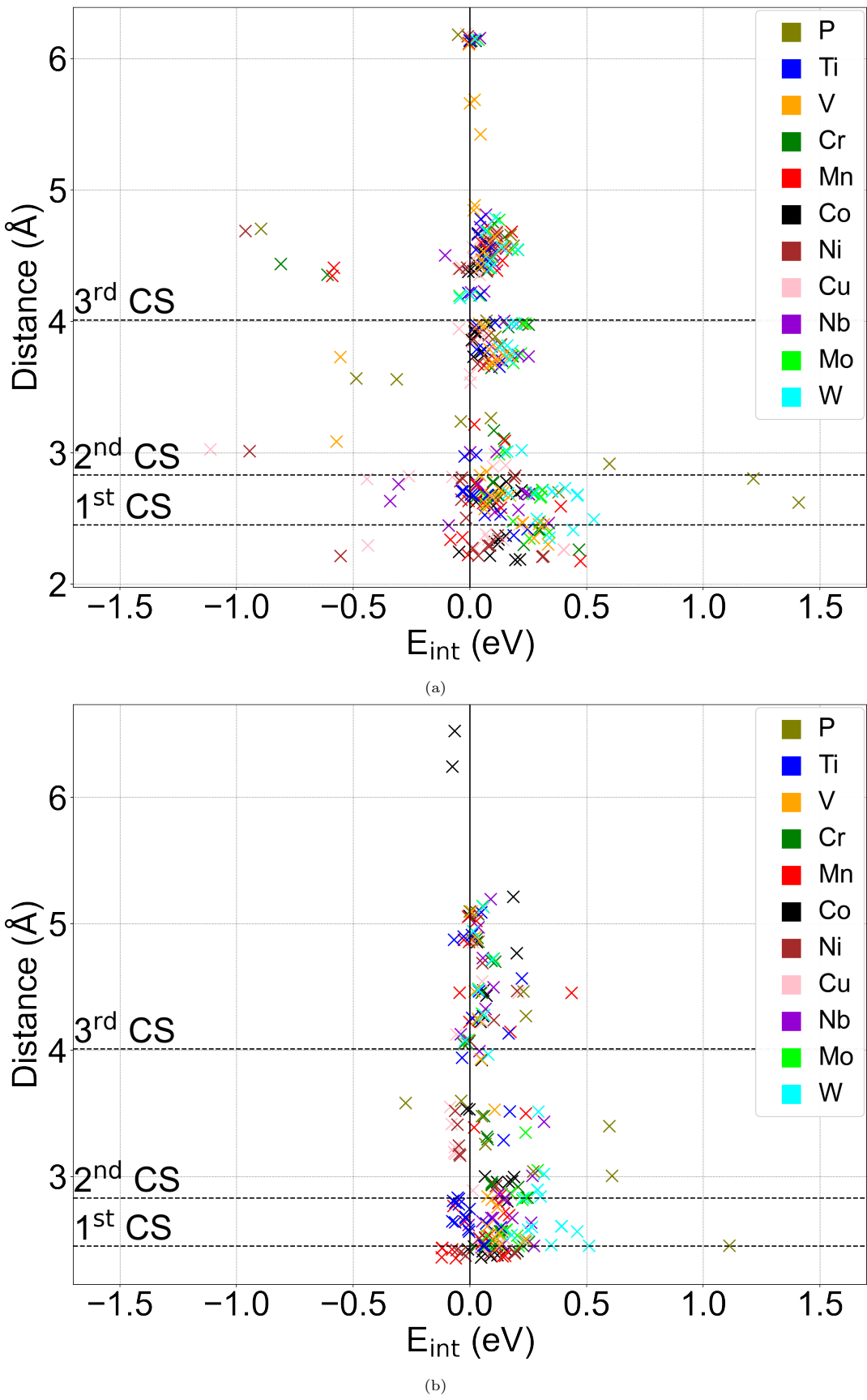
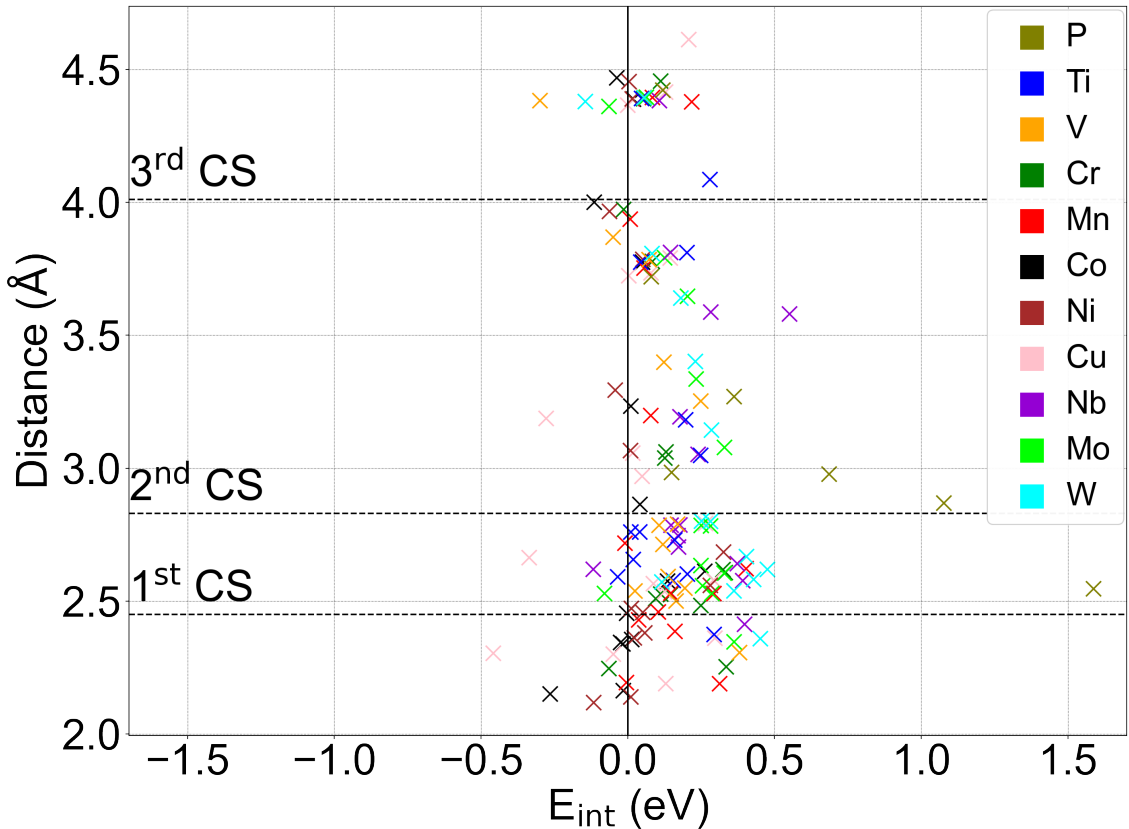
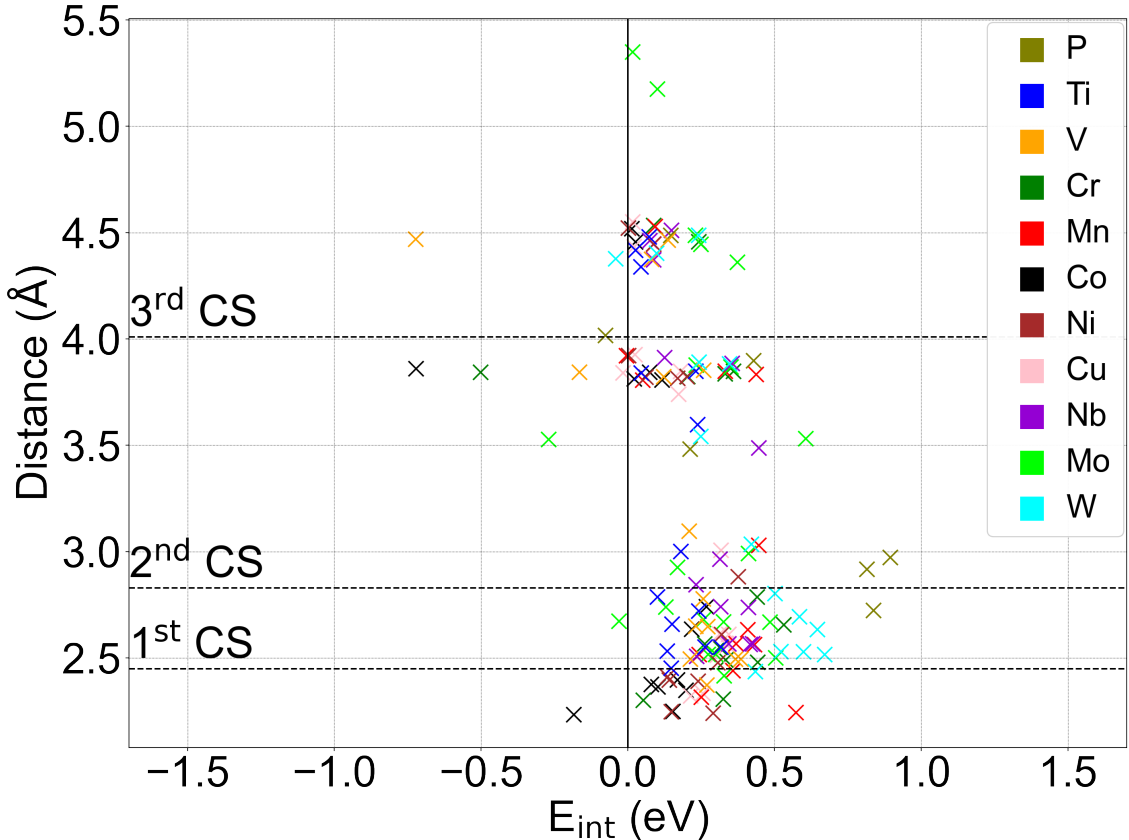


Figure S12: Continued on next page; see next page for caption

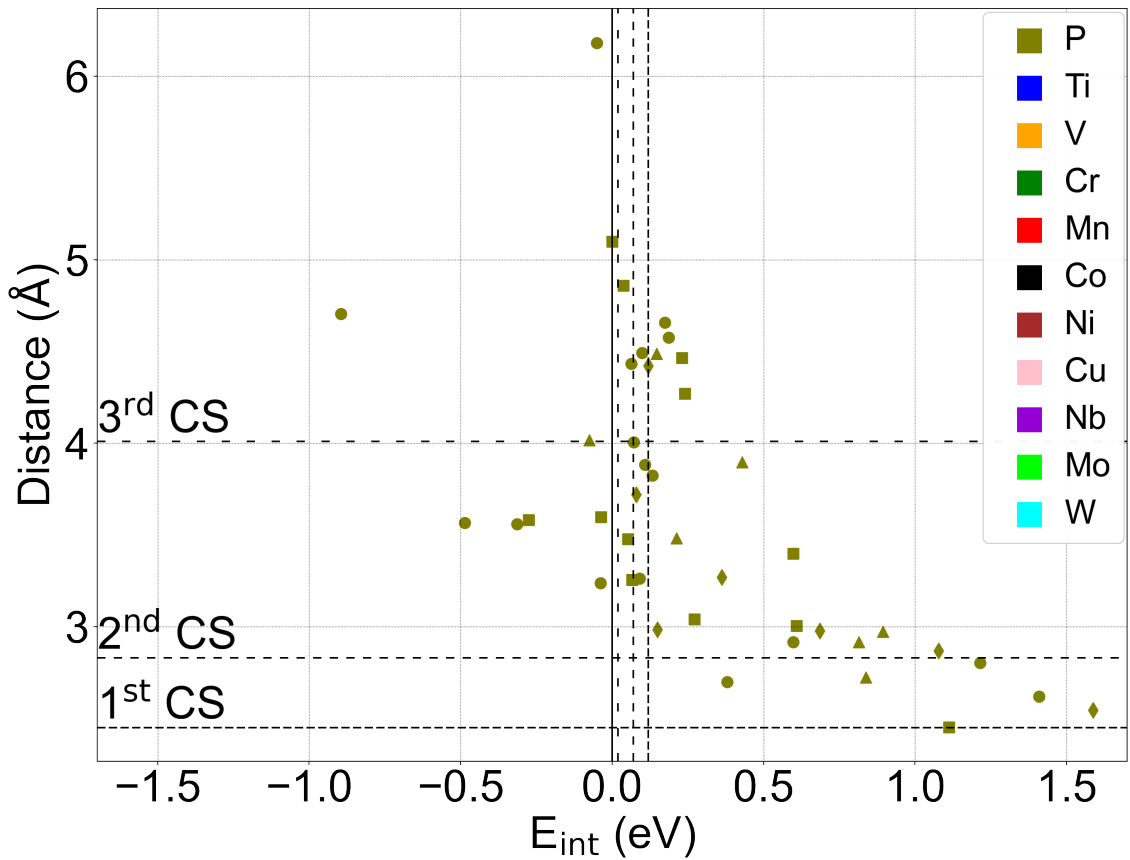


(c)

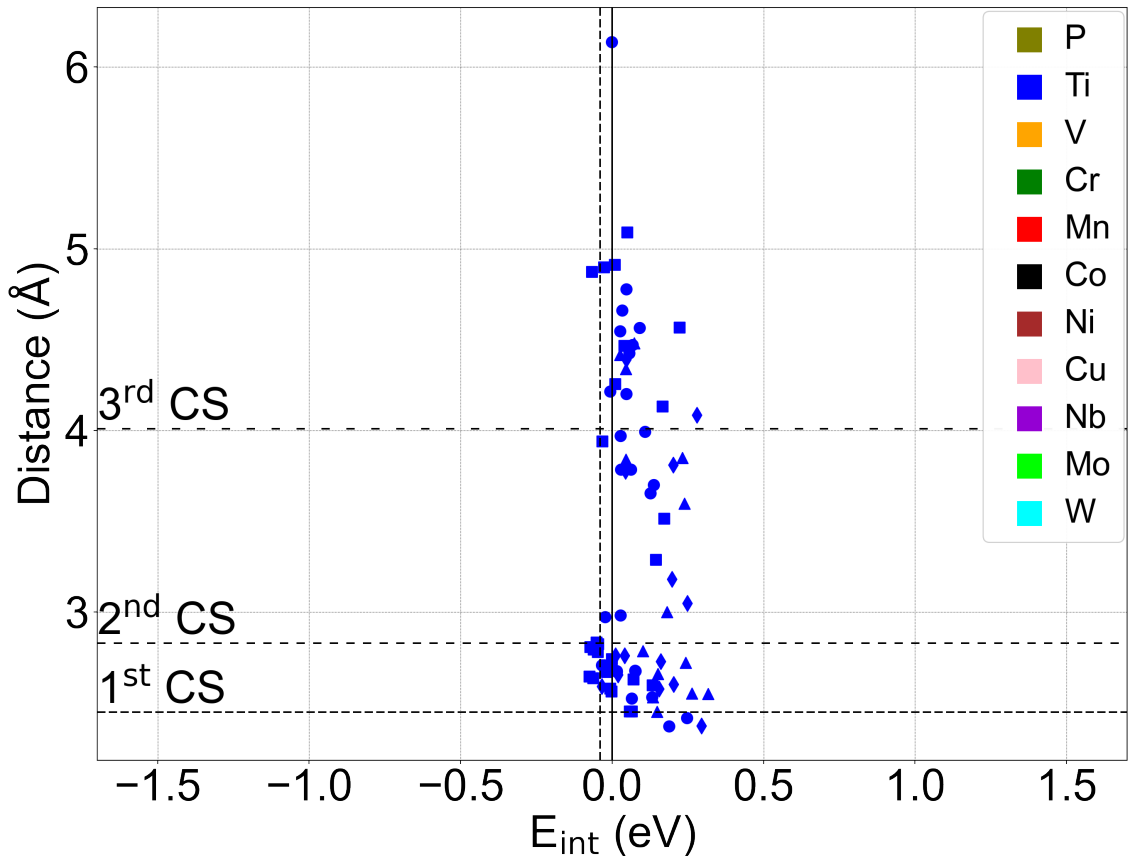


(d)

Figure S12: The interaction energies (E_{int}) are plotted as a function of the P-X solute-solute distance across all co-segregation positions considered. The data are plotted for each of the four GBs: S12a $\Sigma_3(1\bar{1}1)$ S12b $\Sigma_3(1\bar{1}2)$ S12c $\Sigma_9(2\bar{2}1)$ S12d $\Sigma_{11}(3\bar{3}2)$. The horizontal reference lines indicate the distance between solutes for the 1st, 2nd and 3rd coordination shells in the ferritic Fe bulk.

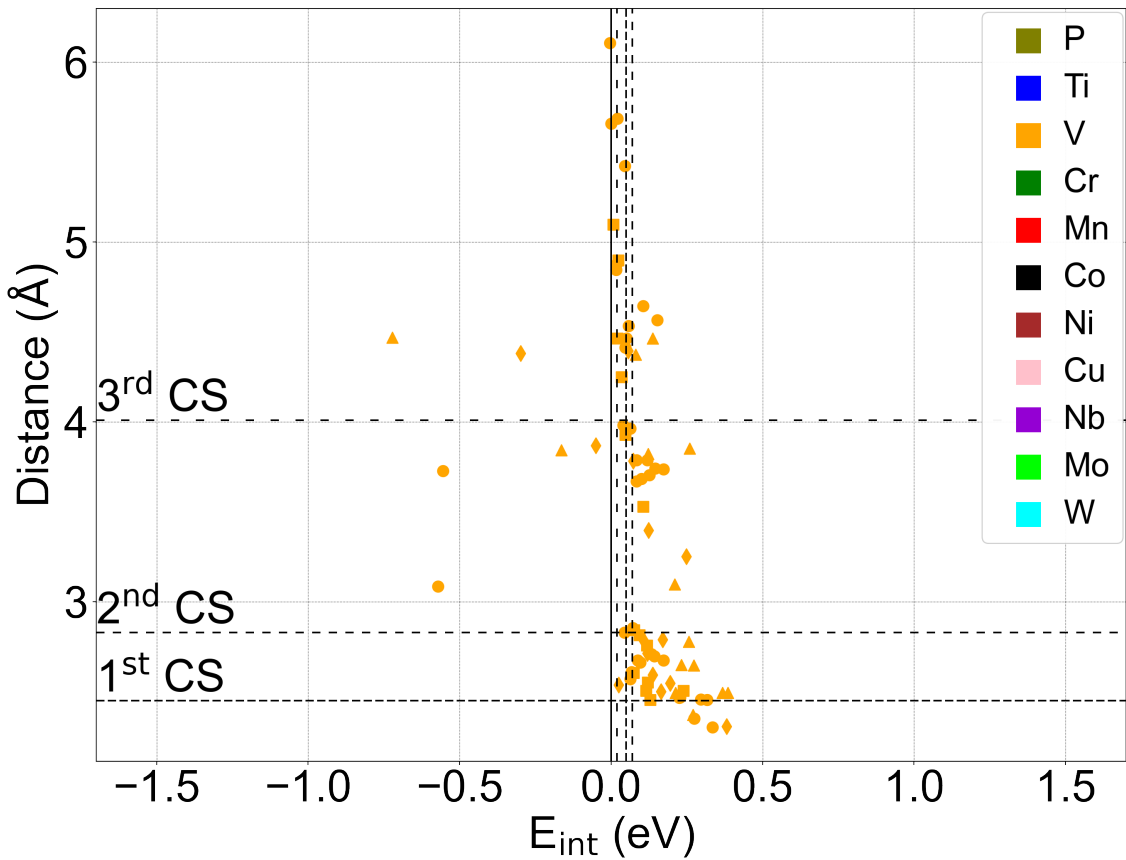


(a)

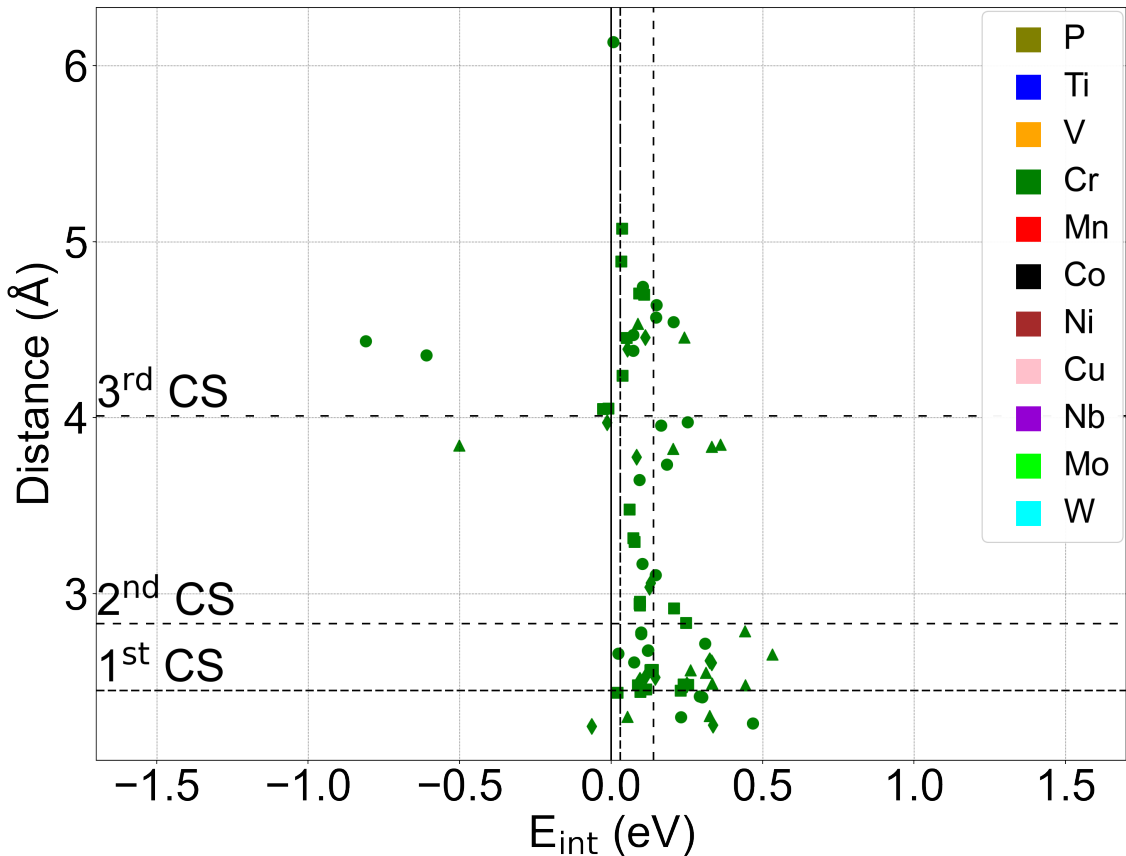


(b)

Figure S13: Continued on next page; see next page for caption

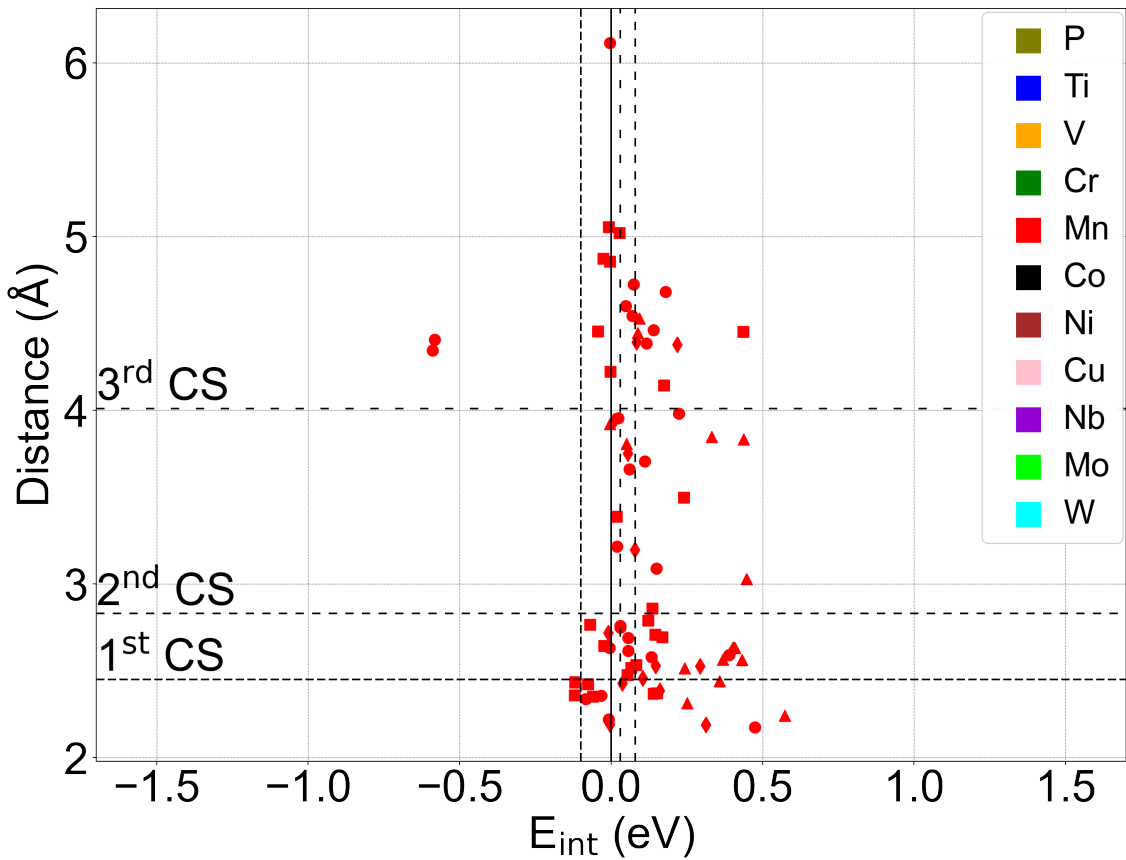


(c)

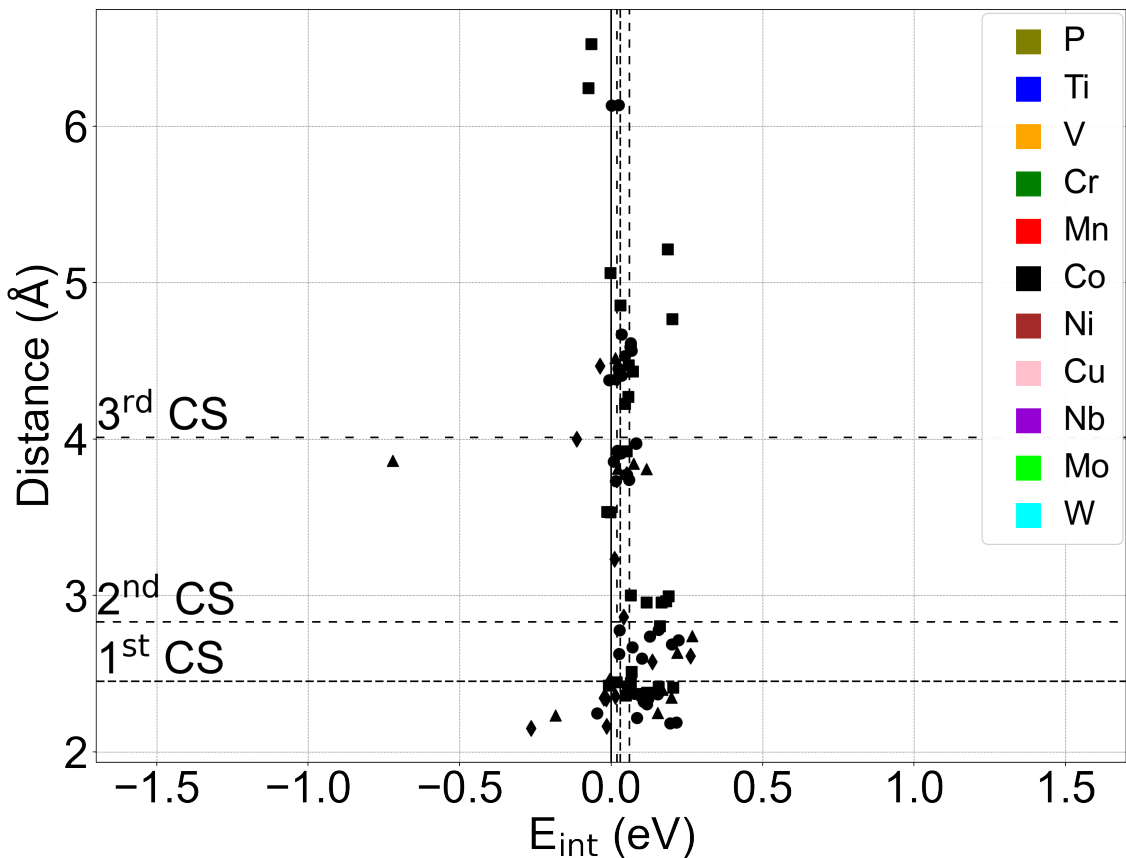


(d)

Figure S13: Continued on next page; see next page for caption

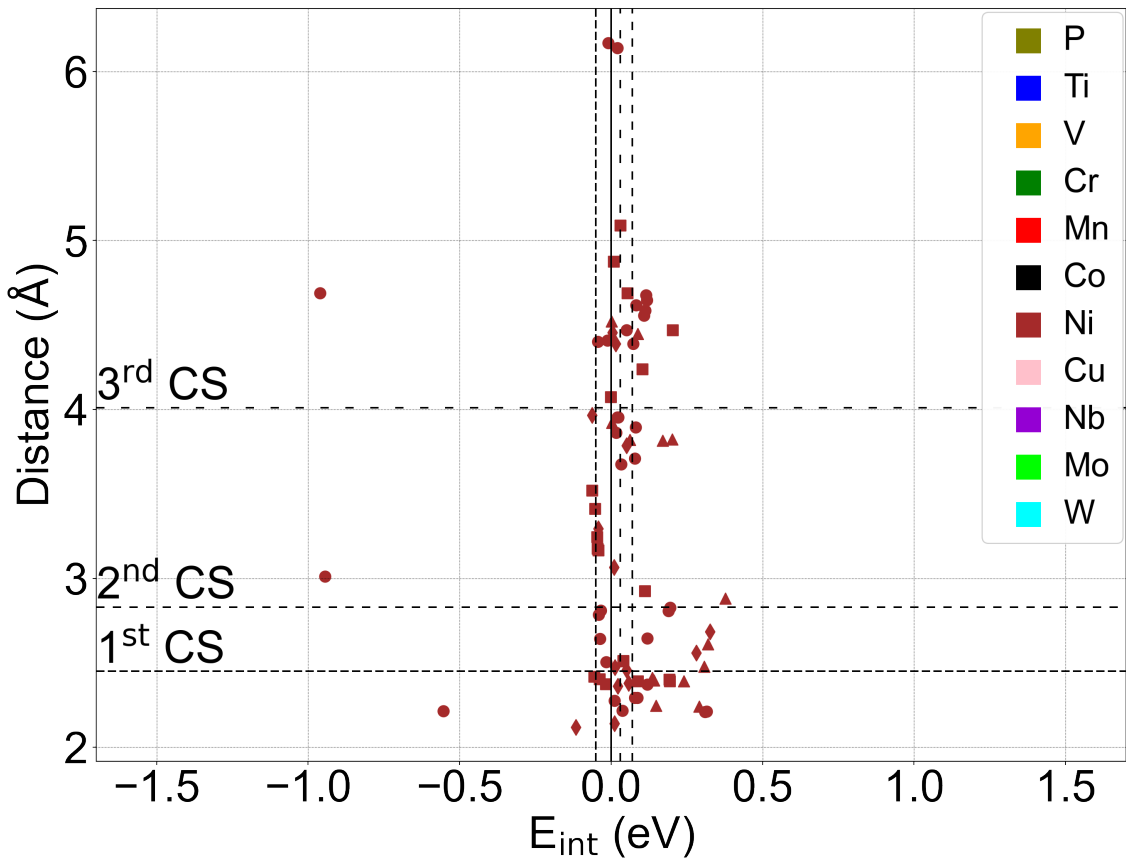


(e)

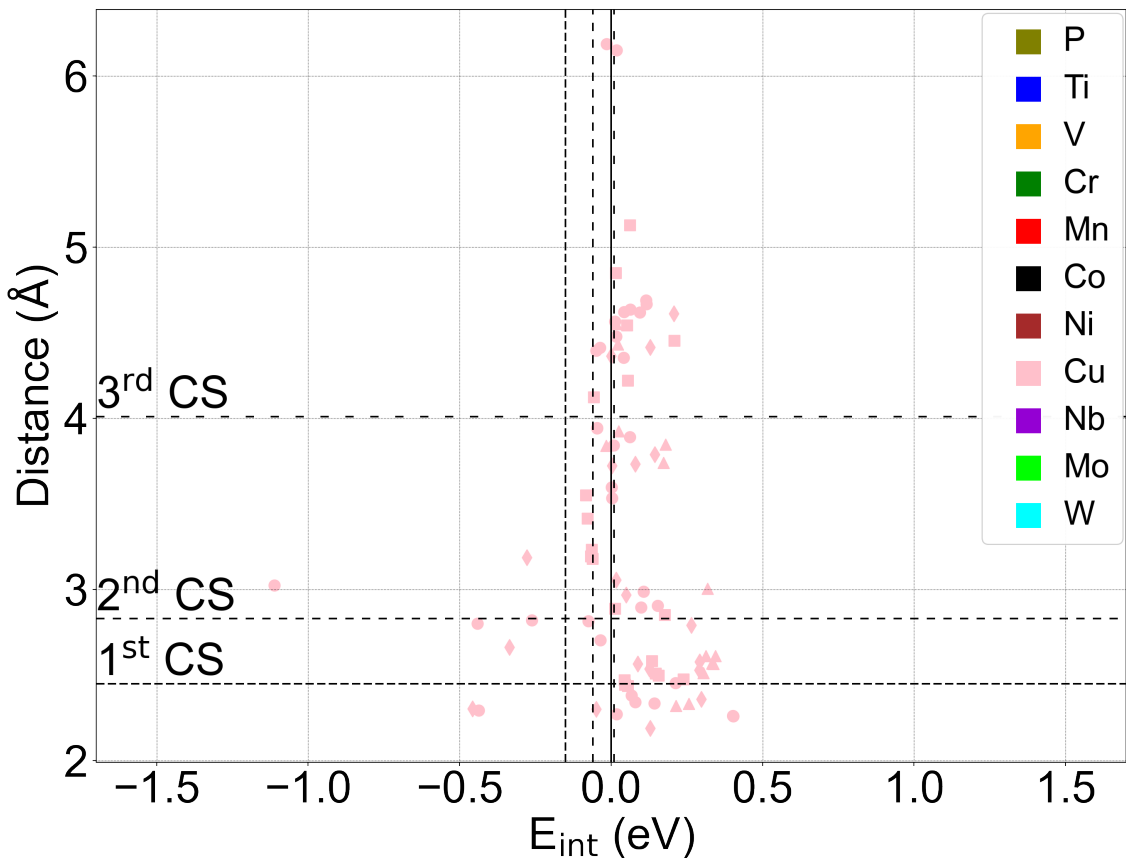


(f)

Figure S13: Continued on next page; see next page for caption

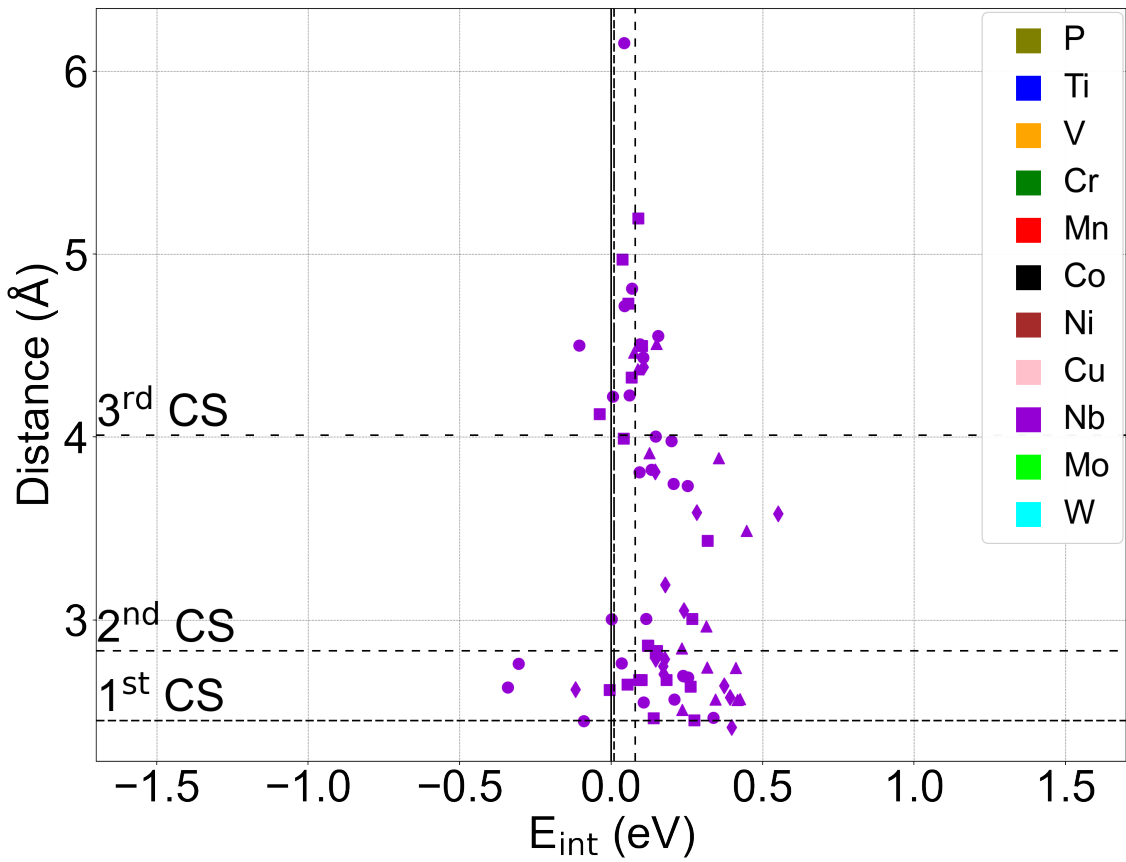


(g)

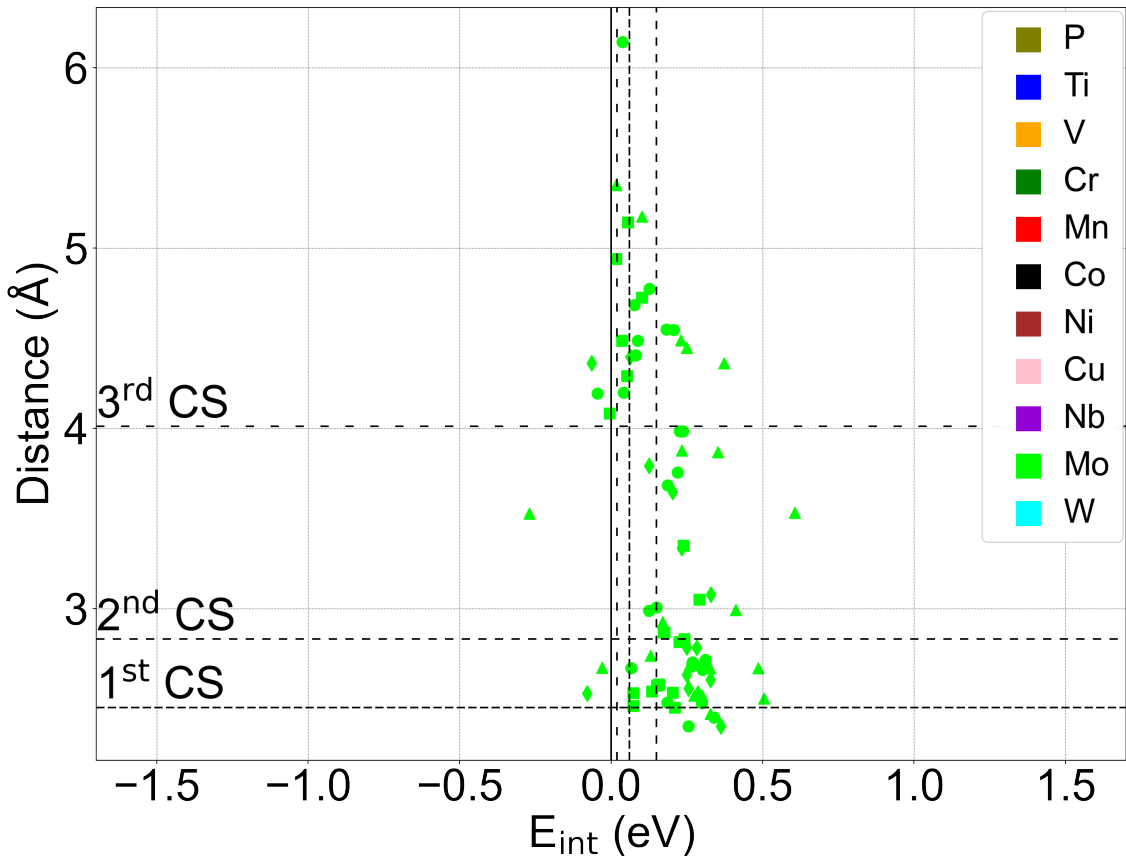


(h)

Figure S13: Continued on next page; see next page for caption



(i)



(j)

Figure S13: Continued on next page; see next page for caption

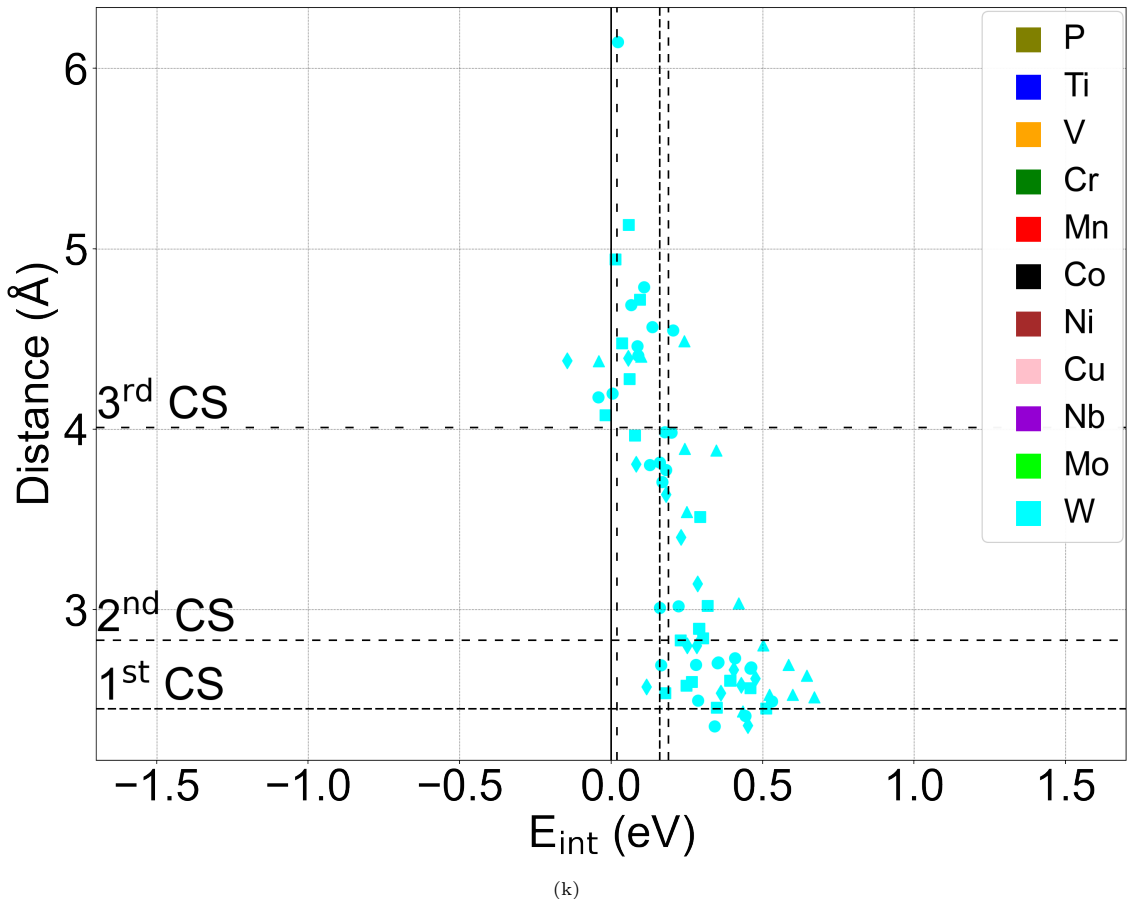


Figure S13: The interaction energies (E_{int}) are plotted as a function of the P-X solute-solute distance across all co-segregation positions considered. The data are plotted for each of the elements: S13a P, S13b Ti, S13c V, S13d Cr, S13e Mn, S13f Co, S13g Ni, S13h Cu, S13i Nb, S13j Mo, S13k W. The horizontal reference lines indicate the distance between solutes for the 1st, 2nd and 3rd coordination shells in the ferritic Fe bulk. The vertical reference lines indicate the bulk P-X interaction energy at the 1st, 2nd and 3rd coordination shells in the bulk, as calculated by Gorbatov et al. in Ref [2].

7.1. P-X Interaction energies in the bulk

In the main text, Fig X. includes reference P-X interaction energies taken from Gorbatov et al.'s study [2]. For convenience of comparison, we tabulate the appropriate reference values in the first, second and third coordination shells for comparison with the values from our study.

P-X bulk solute-solute interaction energies in the bulk (eV)												
Coordination Shell	Distance (Å)	P	Ti	V	Cr	Mn	Co	Ni	Cu	Nb	Mo	W
1	2.45	0.12	-0.04	0.05	0.03	-0.10	0.03	-0.05	-0.15	0.01	0.06	0.16
2	2.83	0.07	0.00	0.07	0.14	0.08	0.06	0.07	-0.06	0.08	0.15	0.19
3	4.01	0.02	0.00	0.02	0.03	0.03	0.02	0.03	0.01	0.01	0.02	0.02

Table S17: The P-X solute-solute interactions that occur in the bulk, as calculated by Gorbatov et al. in his study [2].

8. P-X co-segregation and cohesion

system	$E_{\text{seg}}^{\text{total}}$ (eV)	$E_{\text{seg}}^{\text{inc}}$ (eV)	cleavage plane	η_{RGS} (J/m ²)	$\eta_{\text{RGS}}^{\text{heur}}$ (J/m ²)	η_{rel} (J/m ²)	$\eta_{\text{rel}}^{\text{heur}}$ (J/m ²)	BO cleavage plane	η_{ANSBO} (BO/Å ⁻²)	$\eta_{\text{ANSBO}}^{\text{heur}}$ (BO/Å ⁻²)
Co-34-d-1.1-P-38	-1.262	-1.081	0.521	-0.402	-0.369	-0.258	-0.229	0.521	-0.004	0.002
Cr-36-d-0.0-P-34	-1.222	-1.046	0.496	-0.338	-0.287	-0.189	-0.132	0.496	-0.003	0.001
Cu-34-d-1.1-P-35	-1.701	-1.192	0.463	0.001	-0.588	-0.4	-0.48	0.463	0.004	-0.008
Mn-36-d-0.0-P-34	-1.611	-1.115	0.496	-0.199	-0.222	0.004	0.019	0.496	-0.004	0
Mo-36-d-0.0-P-34	-1.319	-0.878	0.496	-0.043	0.132	-0.03	0.124	0.496	0.007	0.009
Nb-36-d-0.0-P-35	-1.68	-0.908	0.495	-0.296	-0.146	-0.168	-0.031	0.495	-0.007	0.003
Ni-34-d-1.1-P-35	-1.536	-1.123	0.499	0.147	-0.425	-0.195	-0.236	0.499	0.007	-0.004
P-34-d-1.1-Co-38	-1.263	-0.118	0.495	-0.403	-0.369	-0.268	-0.229	0.495	-0.002	0.002
P-34-d-1.1-Cr-36	-1.221	-0.076	0.496	-0.339	-0.287	-0.189	-0.132	0.496	-0.003	0.001
P-34-d-1.1-Cu-30	-1.724	-0.578	0.465	-0.556	-0.588	-0.43	-0.48	0.465	-0.008	-0.008
P-34-d-1.1-Mn-36	-1.611	-0.466	0.496	-0.199	-0.222	0.004	0.019	0.496	-0.004	0
P-34-d-1.1-Mo-36	-1.318	-0.173	0.496	-0.049	0.132	-0.031	0.124	0.496	0.008	0.009
P-34-d-1.1-Nb-37	-1.678	-0.533	0.495	-0.304	-0.146	-0.168	-0.031	0.495	0.007	0.003
P-34-d-1.1-Ni-35	-1.538	-0.393	0.499	0.155	-0.425	-0.194	-0.236	0.463	0.01	-0.004
P-34-d-1.1-P-35	-2.22	-1.074	0.496	-0.639	-0.706	-0.468	-0.412	0.496	0.015	0.008
P-34-d-1.1-Ti-37	-1.609	-0.463	0.496	-0.373	-0.359	-0.183	-0.176	0.496	-0.001	0
P-34-d-1.1-V-40	-1.166	-0.021	0.495	-0.277	-0.226	-0.145	-0.086	0.495	0.003	0.006
P-34-d-1.1-W-36	-1.184	-0.039	0.496	0.203	0.461	0.144	0.349	0.496	0.014	0.015
Ti-36-d-0.0-P-35	-1.609	-1.13	0.496	-0.369	-0.359	-0.183	-0.176	0.496	-0.009	0
V-32-d-1.7-P-38	-1.151	-1.045	0.521	-0.275	-0.226	-0.135	-0.086	0.521	0.001	0.006
W-36-d-0.0-P-34	-1.186	-0.794	0.496	0.208	0.461	0.145	0.349	0.496	0.013	0.015

Table S18: The associated cohesion and segregation data for the co-segregation cases considered for the $\Sigma 3[110](1\bar{1}1)$. The “system” column contains data in the sequence “1st solute”-“1st solute site”-d-“distance to GB”-“2nd solute”-“2nd solute site”. The rest of the columns contain the data for the total segregation energy of the pair ($E_{\text{seg}}^{\text{total}}$), incremental segregation energy of the second solute ($E_{\text{seg}}^{\text{inc}}$), cleavage plane with the minimum rigid work of separation (cleavage plane), the cohesion change enacted by the pair of solutes on the GB calculated by comparing minimum rigid work of separations in the pure and pair-segregated case (η_{RGS}), the heuristic estimate of the rigid cohesion change calculated by the linear sum of both solutes’ individual effects ($\eta_{\text{RGS}}^{\text{heur}}$), the cohesion change enacted by the pair of solutes on the GB calculated by comparing minimum relaxed work of separation in the pure and pair-segregated case (η_{rel}), the corresponding heuristic estimate ($\eta_{\text{RGS}}^{\text{heur}}$), the cleavage plane that yielded the minimum ANSBO (BO cleavage plane), the cohesion change in the ANSBO framework (η_{ANSBO}), and the corresponding heuristic quantity ($\eta_{\text{ANSBO}}^{\text{heur}}$).

system	$E_{\text{seg}}^{\text{total}}$ (eV)	$E_{\text{seg}}^{\text{inc}}$ (eV)	cleavage plane	η_{RGS} (J/m ²)	$\eta_{\text{RGS}}^{\text{heur}}$ (J/m ²)	η_{rel} (J/m ²)	$\eta_{\text{rel}}^{\text{heur}}$ (J/m ²)	BO cleavage plane	η_{ANSBO} (BO/Å ⁻²)	$\eta_{\text{ANSBO}}^{\text{heur}}$ (BO/Å ⁻²)
Co-20-d-2.4-P-25	-0.222	-0.186	0.5	-0.98	-0.909	-1.067	-1.029	0.443	0.008	0.005
Cr-24-d-0.0-P-21	-0.162	-0.098	0.47	-0.886	-0.834	-0.973	-0.967	0.612	0.008	0.006
Cu-24-d-0.0-P-22	-0.494	-0.255	0.497	-1.511	-1.413	-1.49	-1.539	0.526	0.005	-0.002
Mn-22-d-1.2-P-23	-0.483	-0.308	0.471	-0.866	-0.752	-1.035	-0.888	0.527	0.008	0.009
Mo-24-d-0.0-P-20	-0.132	-0.037	0.468	-0.99	-0.562	-1.011	-0.656	0.613	0.009	0.015
Nb-24-d-0.0-P-20	-0.269	-0.118	0.466	-0.951	-0.861	-0.994	-1.106	0.528	0.004	0.005
Ni-24-d-0.0-P-22	-0.383	-0.233	0.497	-1.298	-1.147	-1.283	-1.312	0.497	0.007	-0.002
P-22-d-1.2-Co-27	-0.222	-0.034	0.498	-0.98	-0.909	-1.067	-1.029	0.527	0.002	0.005
P-22-d-1.2-Cr-23	-0.2	-0.012	0.498	-0.874	-0.834	-0.92	-0.967	0.584	0.009	0.006
P-22-d-1.2-Cu-27	-0.5	-0.312	0.498	-0.911	-1.413	-1.103	-1.539	0.526	-0.003	-0.002
P-22-d-1.2-Mn-23	-0.482	-0.293	0.471	-0.833	-0.752	-1.036	-0.888	0.499	0.005	0.009
P-22-d-1.2-Mo-29	-0.188	0.032			-0.562		-0.656			0.015
P-22-d-1.2-Nb-26	-0.316	-0.128	0.494	-0.893	-0.861	-0.957	-1.106	0.526	-0.001	0.005
P-22-d-1.2-Ni-27	-0.39	-0.202	0.498	-0.922	-1.147	-1.062	-1.312	0.527	-0.002	-0.002
P-22-d-1.2-P-18	-0.435	-0.247	0.47	-0.955	-1.918	-1.099	-2.114	0.582	0.01	0.01
P-22-d-1.2-Ti-25	-0.346	-0.157	0.498	-0.875	-0.857	-1.06	-1.112	0.528	0.002	0.005
P-22-d-1.2-V-29	-0.188	0.023			-0.701		-0.871			0.005
P-22-d-1.2-W-30	-0.188	0.031			-0.552		-0.648			0.015
Ti-22-d-1.2-P-25	-0.339	-0.246	0.529	-0.897	-0.857	-1.027	-1.112	0.471	0.008	0.005
W-24-d-0.0-P-19	-0.08	0.009			-0.552		-0.648			0.015

Table S19: The associated cohesion and segregation data for the co-segregation cases considered for the $\Sigma 3[110](1\bar{1}2)$. The “system” column contains data in the sequence “1st solute”-“1st solute site”-d-“distance to GB”-“2nd solute”-“2nd solute site”. The rest of the columns contain the data for the total segregation energy of the pair ($E_{\text{seg}}^{\text{total}}$), incremental segregation energy of the second solute ($E_{\text{seg}}^{\text{inc}}$), cleavage plane with the minimum rigid work of separation (cleavage plane), the cohesion change enacted by the pair of solutes on the GB calculated by comparing minimum rigid work of separations in the pure and pair-segregated case (η_{RGS}), the heuristic estimate of the rigid cohesion change calculated by the linear sum of both solutes’ individual effects ($\eta_{\text{RGS}}^{\text{heur}}$), the cohesion change enacted by the pair of solutes on the GB calculated by comparing minimum relaxed work of separation in the pure and pair-segregated case (η_{rel}), the corresponding heuristic estimate ($\eta_{\text{RGS}}^{\text{heur}}$), the cleavage plane that yielded the minimum ANSBO (BO cleavage plane), the cohesion change in the ANSBO framework (η_{ANSBO}), and the corresponding heuristic quantity ($\eta_{\text{ANSBO}}^{\text{heur}}$).

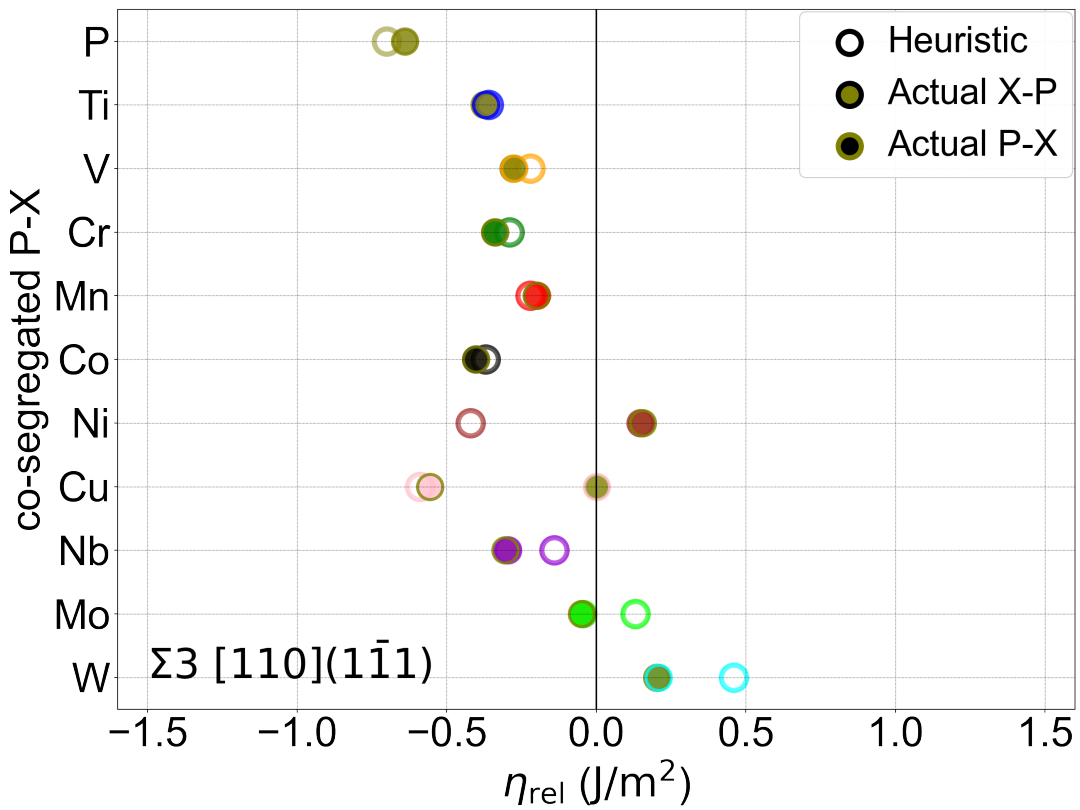
system	$E_{\text{seg}}^{\text{total}}$ (eV)	$E_{\text{seg}}^{\text{inc}}$ (eV)	cleavage plane	η_{RGS} (J/m ²)	$\eta_{\text{RGS}}^{\text{heur}}$ (J/m ²)	η_{rel} (J/m ²)	$\eta_{\text{rel}}^{\text{heur}}$ (J/m ²)	BO cleavage plane	η_{ANSBO} (BO/Å ⁻²)	$\eta_{\text{ANSBO}}^{\text{heur}}$ (BO/Å ⁻²)
Co-36-d-0.0-P-31	-1.307	-1.17	0.479	-0.236	0.058	-0.08	0.088	0.501	-0.006	-0.002
Cr-36-d-0.0-P-31	-1.182	-0.969	0.479	-0.246	0.178	-0.064	0.212	0.502	-0.004	0.002
Cu-33-d-1.2-P-36	-1.879	-1.241	0.502	-0.556	-0.48	-0.309	-0.23	0.48	-0.019	-0.022
Mn-36-d-0.0-P-31	-1.447	-0.91	0.48	-0.028	0.41	0.085	0.251	0.5	-0.007	0
Mo-34-d-0.0-P-36	-1.503	-1.078	0.503	0.429	0.555	0.316	0.367	0.48	0.007	0.006
Nb-34-d-0.0-P-36	-2.184	-1.181	0.502	0.281	0.361	0.405	0.408	0.479	0.007	0.006
Ni-36-d-0.0-P-31	-1.452	-1.021	0.479	-0.294	0.004	-0.165	0.015	0.5	-0.015	-0.003
P-36-d-0.0-Co-33	-1.446	-0.087	0.502	-0.136	0.058	0.053	0.088	0.48	-0.005	-0.002
P-36-d-0.0-Cr-33	-1.407	-0.047	0.502	-0.19	0.178	0.075	0.212	0.502	-0.007	0.002
P-36-d-0.0-Cu-33	-1.871	-0.511	0.502	-0.553	-0.48	-0.315	-0.23	0.48	-0.017	-0.022
P-36-d-0.0-Mn-33	-1.72	-0.361	0.502	-0.022	0.41	0.131	0.251	0.502	-0.005	0
P-36-d-0.0-Mo-34	-1.502	-0.142	0.503	0.424	0.555	0.315	0.367	0.48	0.007	0.006
P-36-d-0.0-Nb-34	-2.185	-0.826	0.502	0.281	0.361	0.405	0.408	0.479	0.008	0.006
P-36-d-0.0-Ni-33	-1.734	-0.374	0.502	-0.274	0.004	-0.022	0.015	0.48	-0.011	-0.003
P-36-d-0.0-P-33	-2.007	-0.648	0.502	-0.652	-0.066	-0.537	-0.062	0.49	0.021	-0.001
P-36-d-0.0-Ti-34	-2.056	-0.697	0.502	0.163	0.177	0.313	0.27	0.48	0.005	0.002
P-36-d-0.0-V-29	-1.359	0.042			0.264		0.147			0.003
P-36-d-0.0-W-34	-1.385	-0.026	0.503	0.713	0.739	0.41	0.265	0.48	0.01	0.008
Ti-34-d-0.0-P-36	-2.056	-1.318	0.502	0.163	0.177	0.312	0.27	0.48	0.005	0.002
V-34-d-0.0-P-36	-1.34	-1.222	0.503	0.213	0.264	0.183	0.147	0.48	0.005	0.003
W-34-d-0.0-P-36	-1.385	-1.077	0.503	0.714	0.739	0.41	0.265	0.48	0.01	0.008

Table S20: The associated cohesion and segregation data for the co-segregation cases considered for the Σ9[110](2̄2̄1). The “system” column contains data in the sequence “1st solute”-“1st solute site”-d-“distance to GB”-“2nd solute”-“2nd solute site”. The rest of the columns contain the data for the total segregation energy of the pair ($E_{\text{seg}}^{\text{total}}$), incremental segregation energy of the second solute ($E_{\text{seg}}^{\text{inc}}$), cleavage plane with the minimum rigid work of separation (cleavage plane), the cohesion change enacted by the pair of solutes on the GB calculated by comparing minimum rigid work of separations in the pure and pair-segregated case (η_{RGS}), the heuristic estimate of the rigid cohesion change calculated by the linear sum of both solutes’ individual effects ($\eta_{\text{RGS}}^{\text{heur}}$), the cohesion change enacted by the pair of solutes on the GB calculated by comparing minimum relaxed work of separation in the pure and pair-segregated case (η_{rel}), the corresponding heuristic estimate ($\eta_{\text{RGS}}^{\text{heur}}$), the cleavage plane that yielded the minimum ANSBO (BO cleavage plane), the cohesion change in the ANSBO framework (η_{ANSBO}), and the corresponding heuristic quantity ($\eta_{\text{ANSBO}}^{\text{heur}}$).

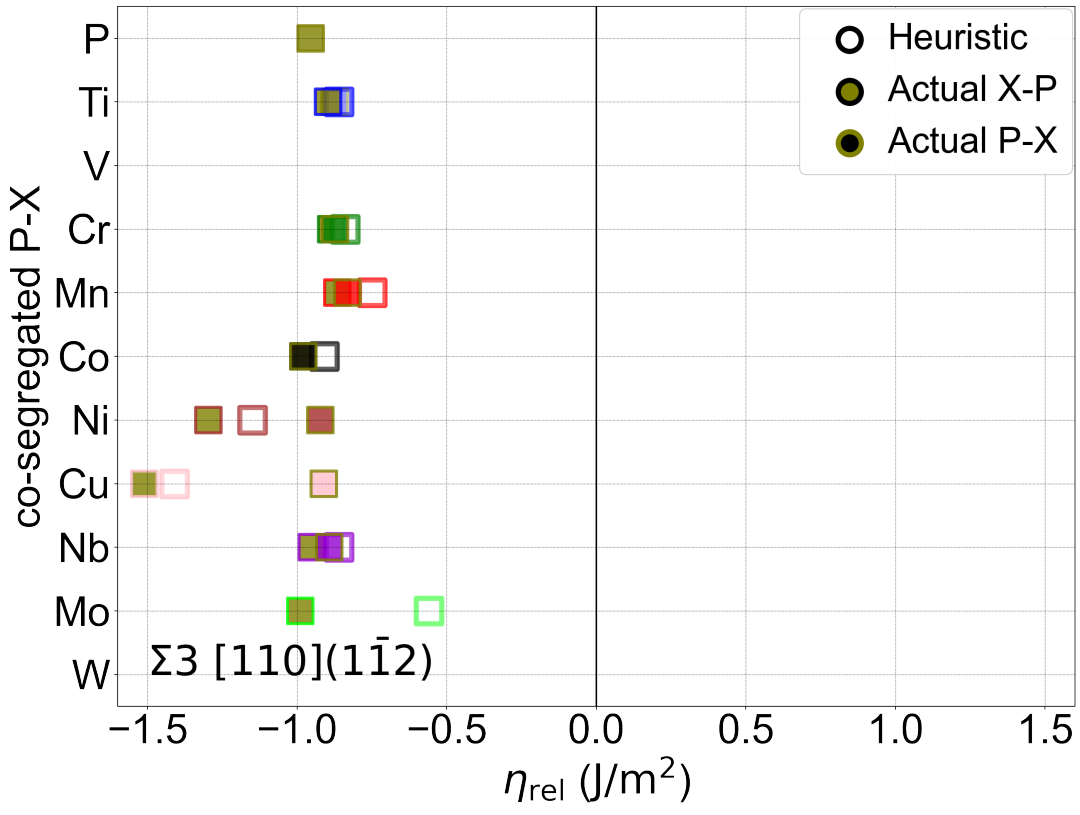
system	$E_{\text{seg}}^{\text{total}}$ (eV)	$E_{\text{seg}}^{\text{inc}}$ (eV)	cleavage plane	η_{RGS} (J/m ²)	$\eta_{\text{RGS}}^{\text{heur}}$ (J/m ²)	η_{rel} (J/m ²)	$\eta_{\text{rel}}^{\text{heur}}$ (J/m ²)	BO cleavage plane	η_{ANSBO} (BO/Å ⁻²)	$\eta_{\text{ANSBO}}^{\text{heur}}$ (BO/Å ⁻²)
Co-21-d-0.0-P-20	-1.046	-0.898	0.499	-0.4	-0.21	-0.325	-0.218	0.488	0.014	0.008
Cr-21-d-0.0-P-20	-0.954	-0.665	0.501	-0.462	-0.034	-0.345	-0.036	0.501	0.014	0.011
Cu-21-d-0.0-P-20	-1.385	-0.641	0.5	-0.885	-0.577	-0.855	-0.539	0.5	-0.001	0.002
Mn-21-d-0.0-P-20	-1.226	-0.609	0.5	-0.147	0.238	-0.318	0.033	0.548	0.003	0.013
Mo-19-d-1.5-P-20	-1.243	-0.704	0.503	0.294	0.415	0.108	0.299	0.427	0.023	0.019
Nb-22-d-0.0-P-21	-1.555	-0.643	0.5	-0.149	0.111	-0.039	0.196	0.475	0.017	0.019
Ni-21-d-0.0-P-20	-1.234	-0.671	0.5	-0.647	-0.266	-0.5	-0.208	0.548	0.002	0.005
P-21-d-0.0-Co-20	-1.049	-0.022	0.501	-0.404	-0.21	-0.322	-0.218	0.501	0.005	0.008
P-21-d-0.0-Cr-15	-1.028	0.055								
P-21-d-0.0-Cu-20	-1.375	-0.348	0.5	-0.906	-0.577	-0.863	-0.539	0.5	-0.009	0.002
P-21-d-0.0-Mn-20	-1.221	-0.194	0.501	-0.187	0.238	-0.322	0.033	0.501	0.005	0.013
P-21-d-0.0-Mo-22	-1.244	-0.217	0.501	0.298	0.415	0.109	0.299	0.475	0.017	0.019
P-21-d-0.0-Nb-22	-1.554	-0.527	0.5	-0.158	0.111	-0.039	0.196	0.475	0.018	0.019
P-21-d-0.0-Ni-20	-1.274	-0.246	0.5	-0.574	-0.266	-0.466	-0.208	0.5	0	0.005
P-21-d-0.0-P-16	-1.204	-0.176	0.451	-0.359	-0.736	-0.112	-0.756	0.487	0.005	0.021
P-21-d-0.0-Ti-22	-1.376	-0.349	0.523	-0.404	-0.117	-0.237	-0.016	0.476	0.015	0.01
P-21-d-0.0-V-15	-1.028	0.009								
P-21-d-0.0-W-15	-1.028	0.033								
Ti-22-d-0.0-P-21	-1.376	-0.751	0.523	-0.402	-0.117	-0.237	-0.016	0.475	0.015	0.01
V-22-d-0.0-P-16	-1.023	-0.823	0.451	-0.349	0.08	-0.35	-0.033	0.549	0.015	0.012
W-22-d-0.0-P-21	-0.972	-0.47	0.501	0.665	0.659	0.28	0.186	0.475	0.019	0.024

Table S21: The associated cohesion and segregation data for the co-segregation cases considered for the Σ11[110](332). The “system” column contains data in the sequence “1st solute”-“1st solute site”-d-“distance to GB”-“2nd solute”-“2nd solute site”. The rest of the columns contain the data for the total segregation energy of the pair ($E_{\text{seg}}^{\text{total}}$), incremental segregation energy of the second solute ($E_{\text{seg}}^{\text{inc}}$), cleavage plane with the minimum rigid work of separation (cleavage plane), the cohesion change enacted by the pair of solutes on the GB calculated by comparing minimum rigid work of separations in the pure and pair-segregated case (η_{RGS}), the heuristic estimate of the rigid cohesion change calculated by the linear sum of both solutes’ individual effects ($\eta_{\text{RGS}}^{\text{heur}}$), the cohesion change enacted by the pair of solutes on the GB calculated by comparing minimum relaxed work of separation in the pure and pair-segregated case (η_{rel}), the corresponding heuristic estimate ($\eta_{\text{RGS}}^{\text{heur}}$), the cleavage plane that yielded the minimum ANSBO (BO cleavage plane), the cohesion change in the ANSBO framework (η_{ANSBO}), and the corresponding heuristic quantity ($\eta_{\text{ANSBO}}^{\text{heur}}$).

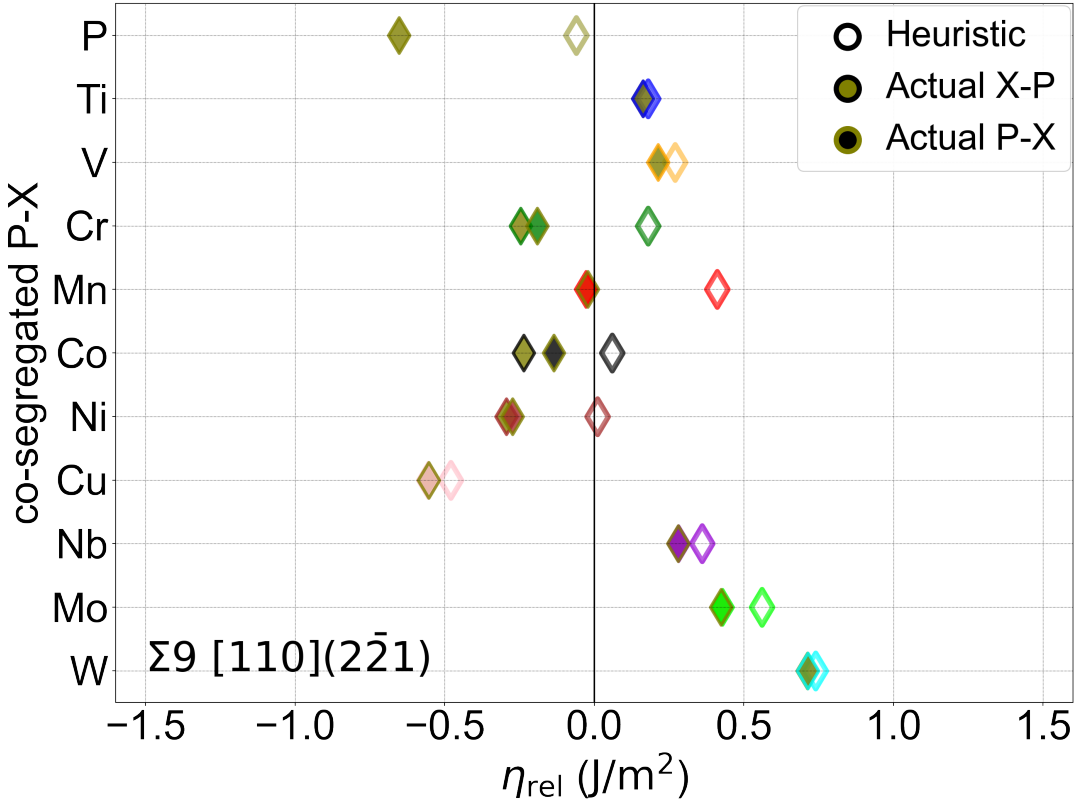
9. P-X co-segregation and cohesion: Heuristic Analysis



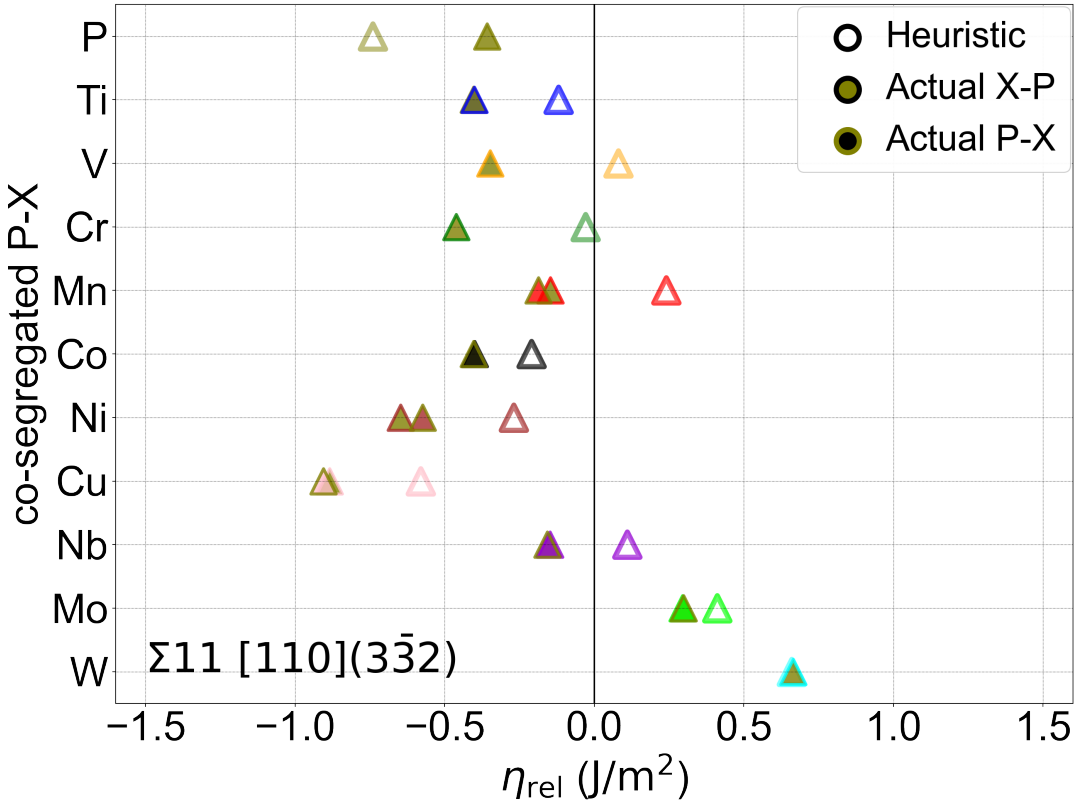
(a)



(b)

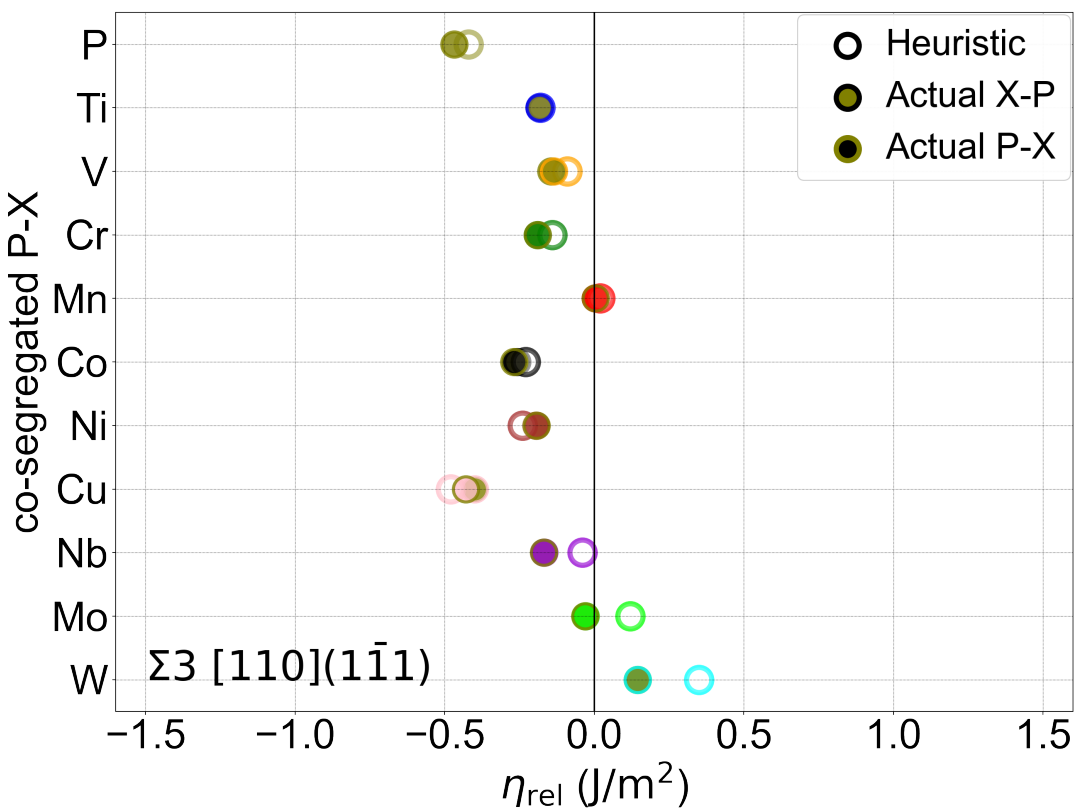


(c)

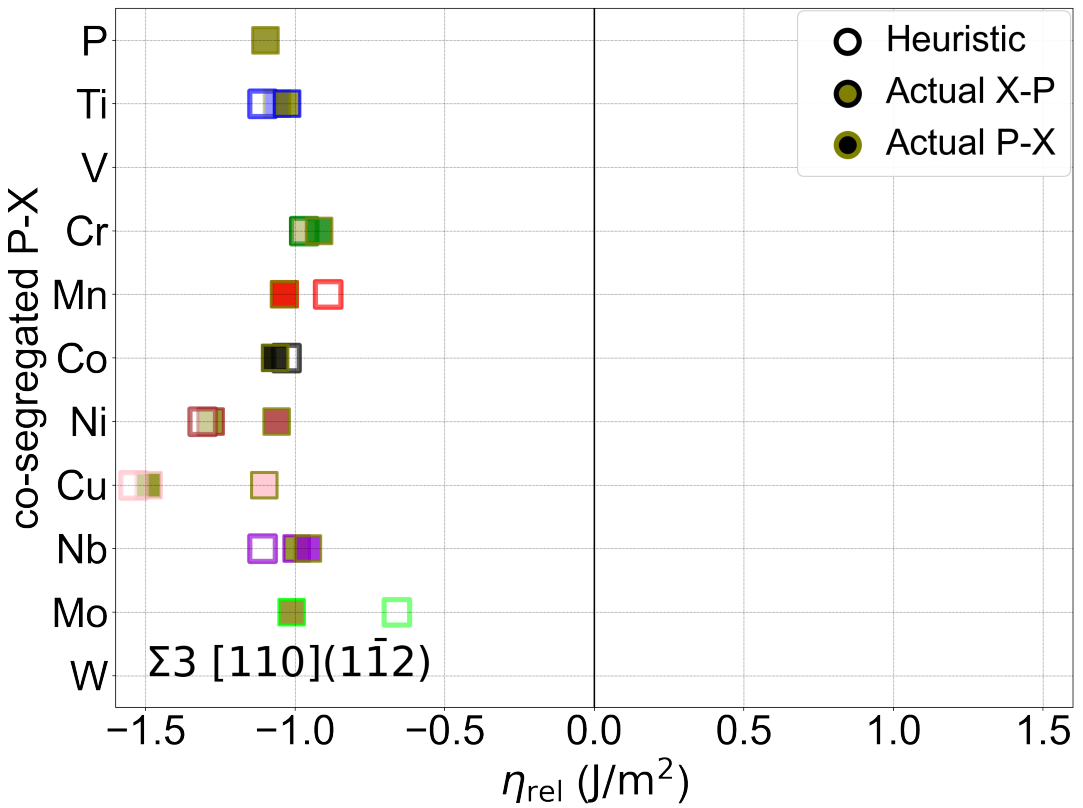


(d)

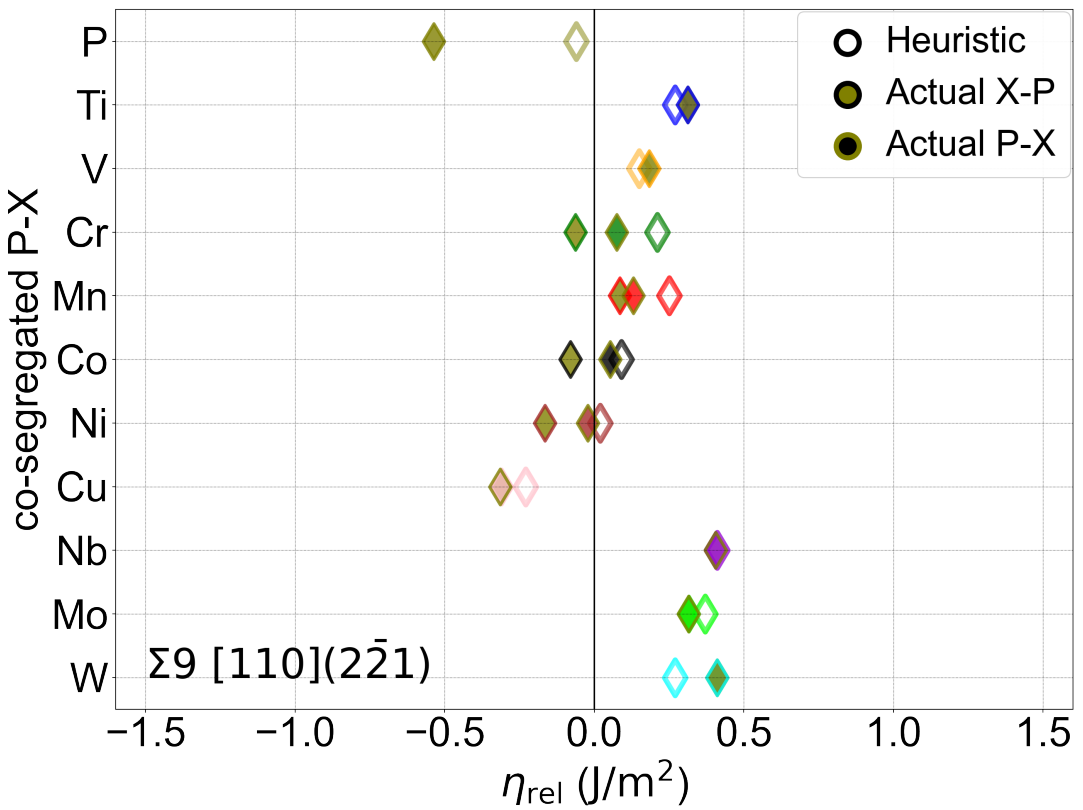
Figure S14: The heuristic linear sum of the individual solutes effects on GB cohesion are compared with their actual computed effect on cohesion, for the cohesive quantity of η_{RGS} . These are plotted for the S14a $\Sigma 3(1\bar{1}1)$ S14b $\Sigma 3(1\bar{1}2)$ S14c $\Sigma 9(2\bar{2}1)$ S14d and $\Sigma 11(3\bar{3}2)$ GBs.



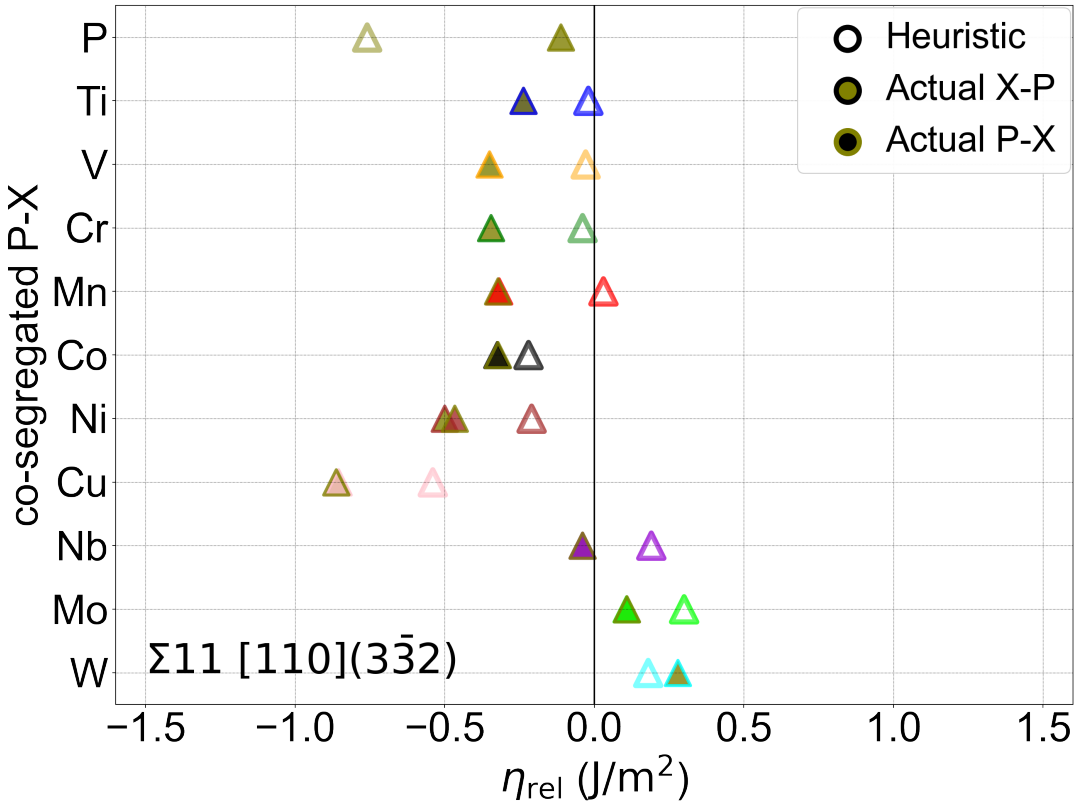
(a)



(b)

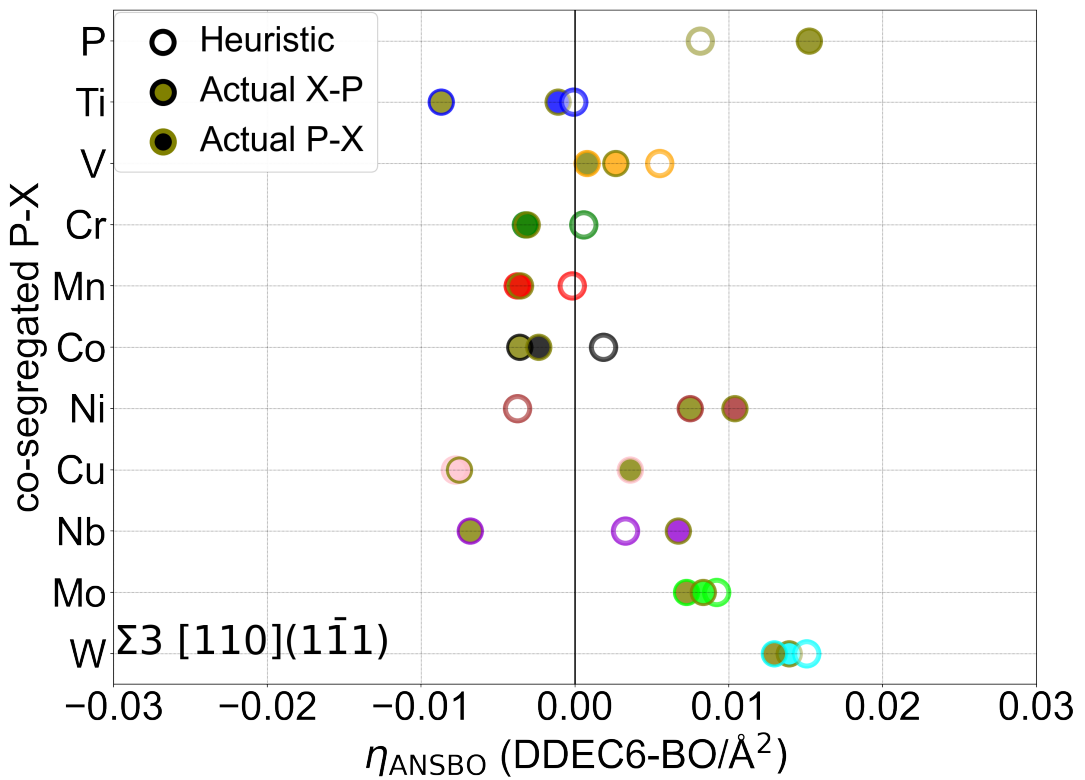


(c)

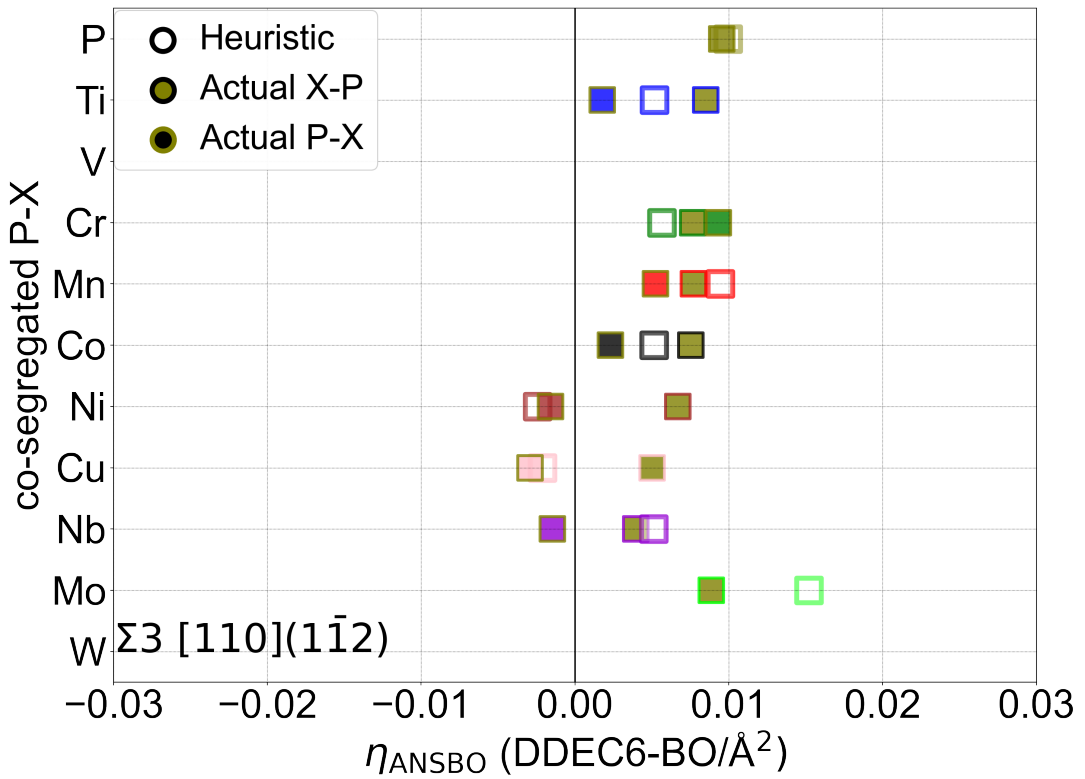


(d)

Figure S15: The heuristic linear sum of the individual solutes effects on GB cohesion are compared with their actual computed effect on cohesion, for the cohesive quantity of η_{rel} . These are plotted for the S15a $\Sigma 3(1\bar{1}1)$ S15b $\Sigma 3(1\bar{1}2)$ S15c $\Sigma 9(2\bar{2}1)$ S15d and $\Sigma 11(3\bar{3}2)$ GBs.



(a)



(b)

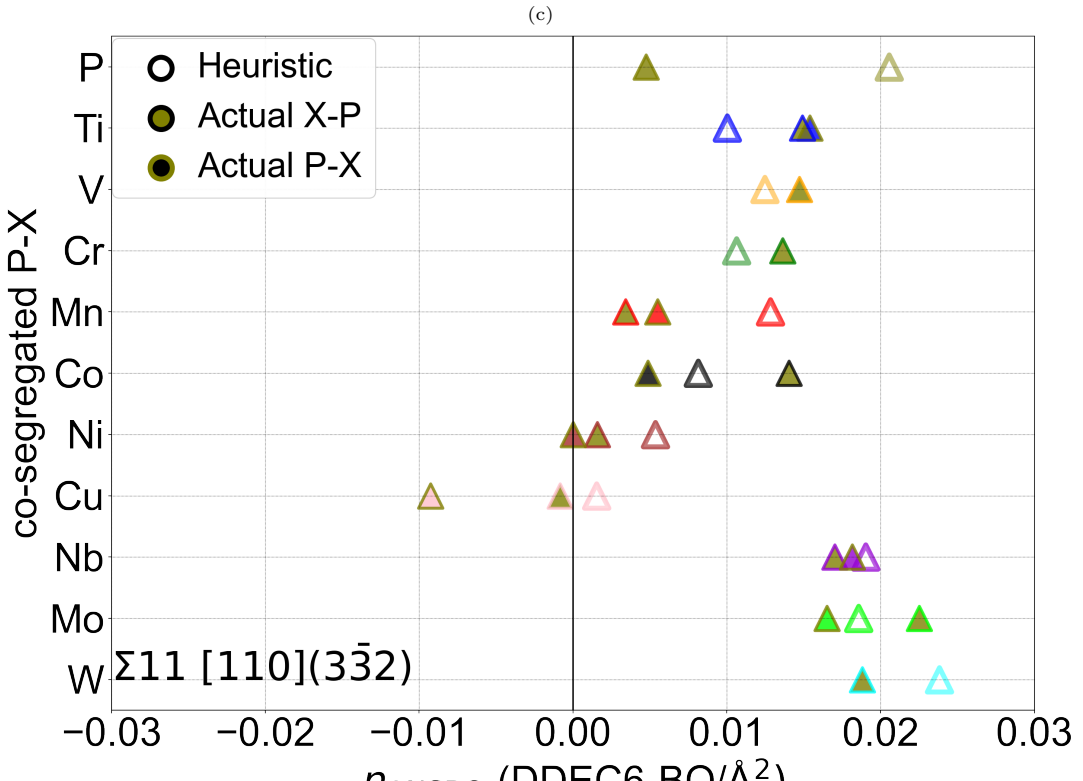
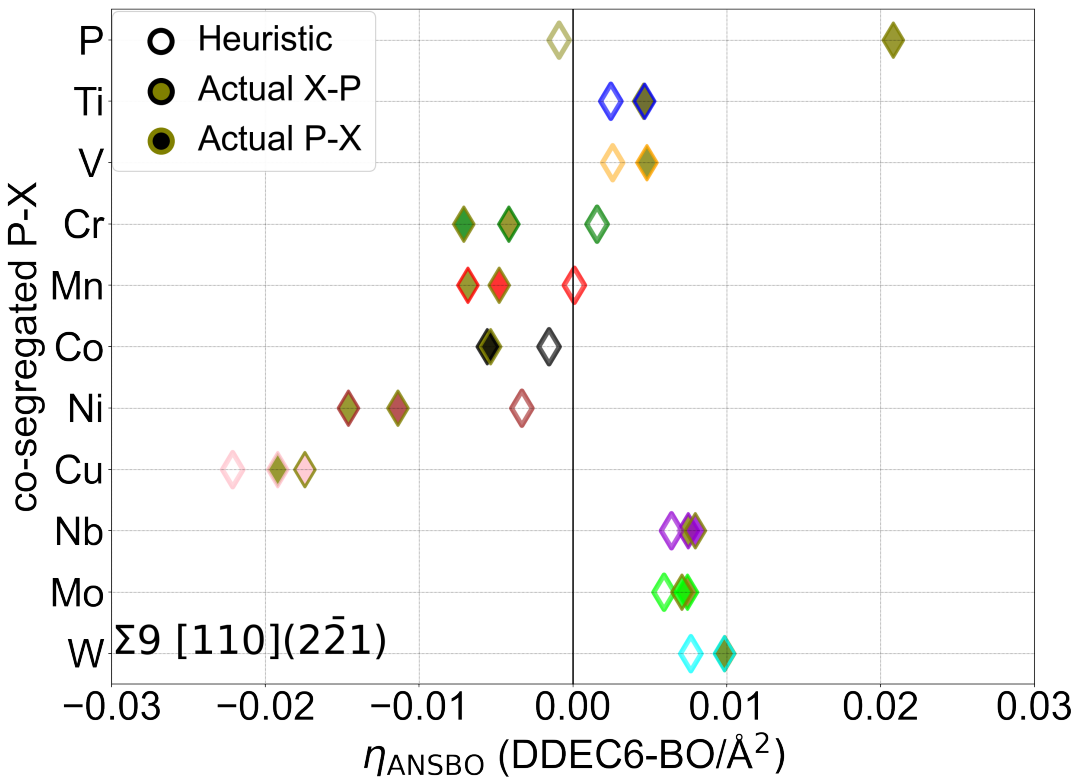
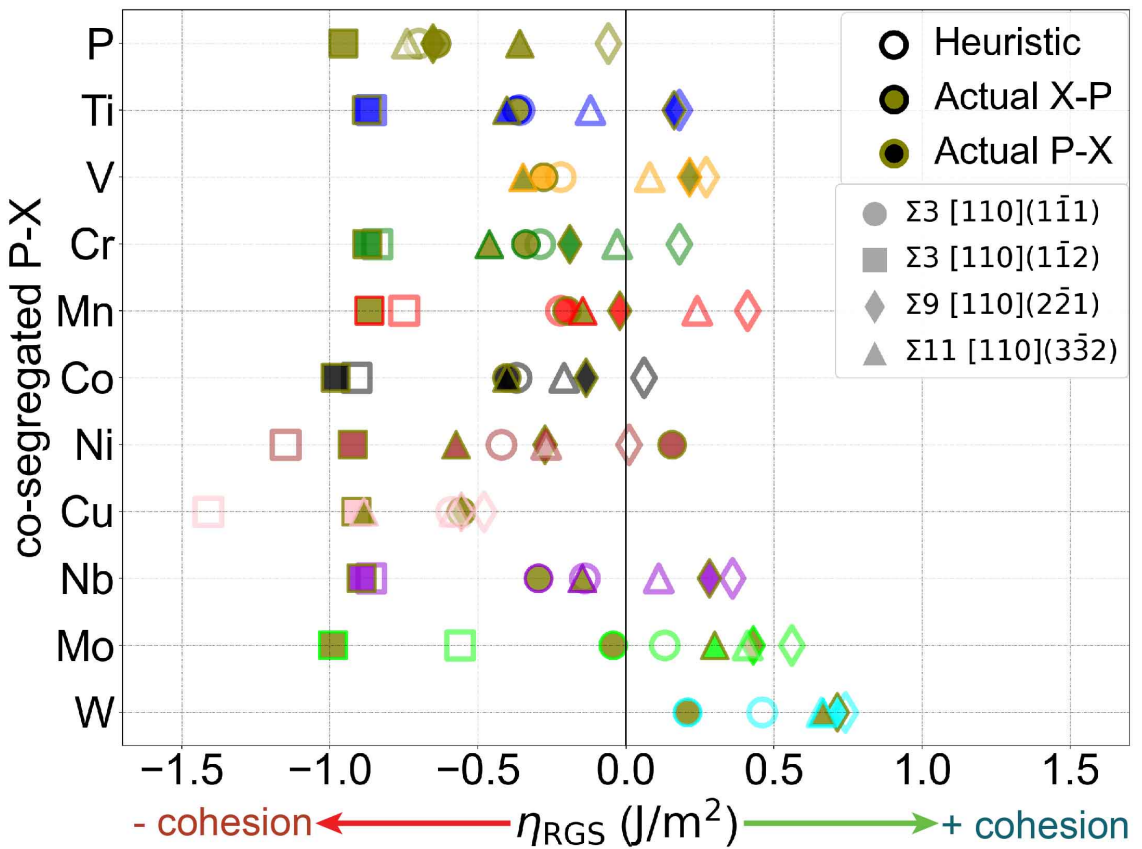
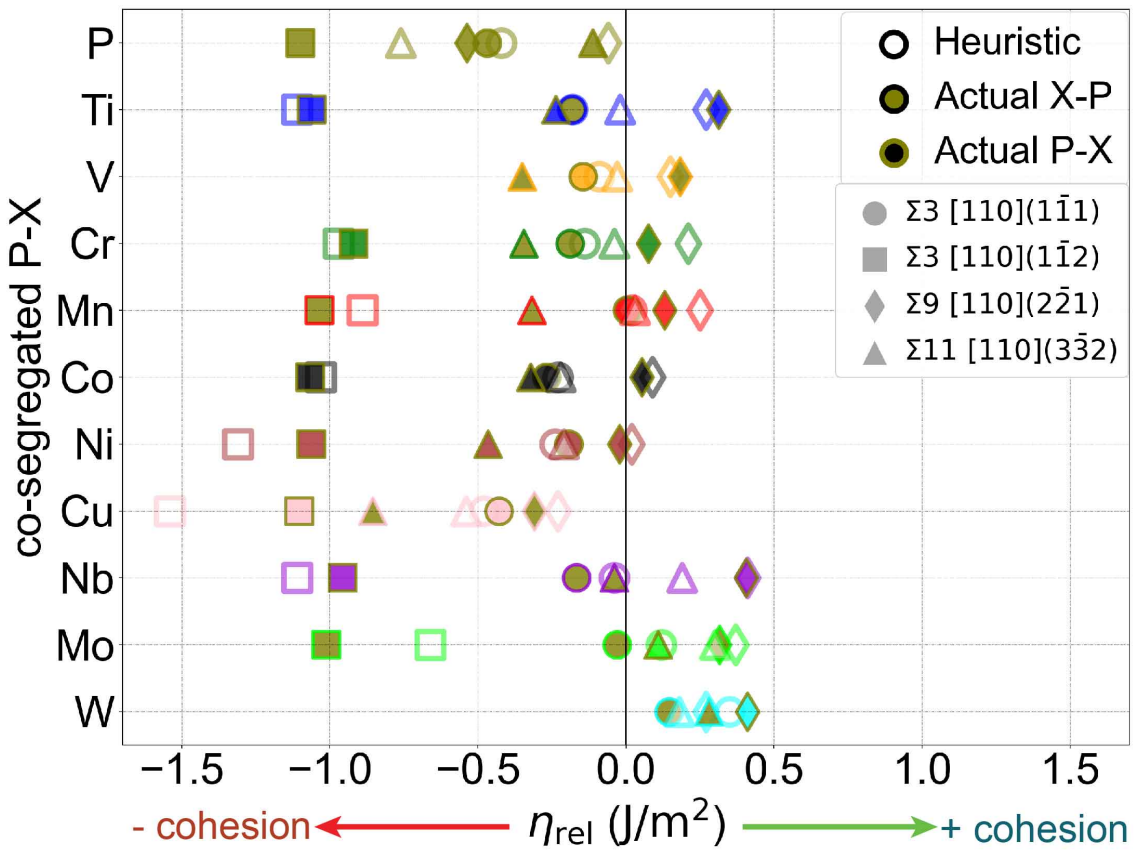


Figure S16: The heuristic linear sum of the individual solutes effects on GB cohesion are compared with their actual computed effect on cohesion, for the cohesive quantity of η_{ANSBO} . These are plotted for the S16a $\Sigma 3(1\bar{1}1)$ S16b $\Sigma 3(1\bar{1}2)$ S16c $\Sigma 9(2\bar{2}1)$ S16d and $\Sigma 11(3\bar{3}\bar{2})$ GBs.



(a)



(b)

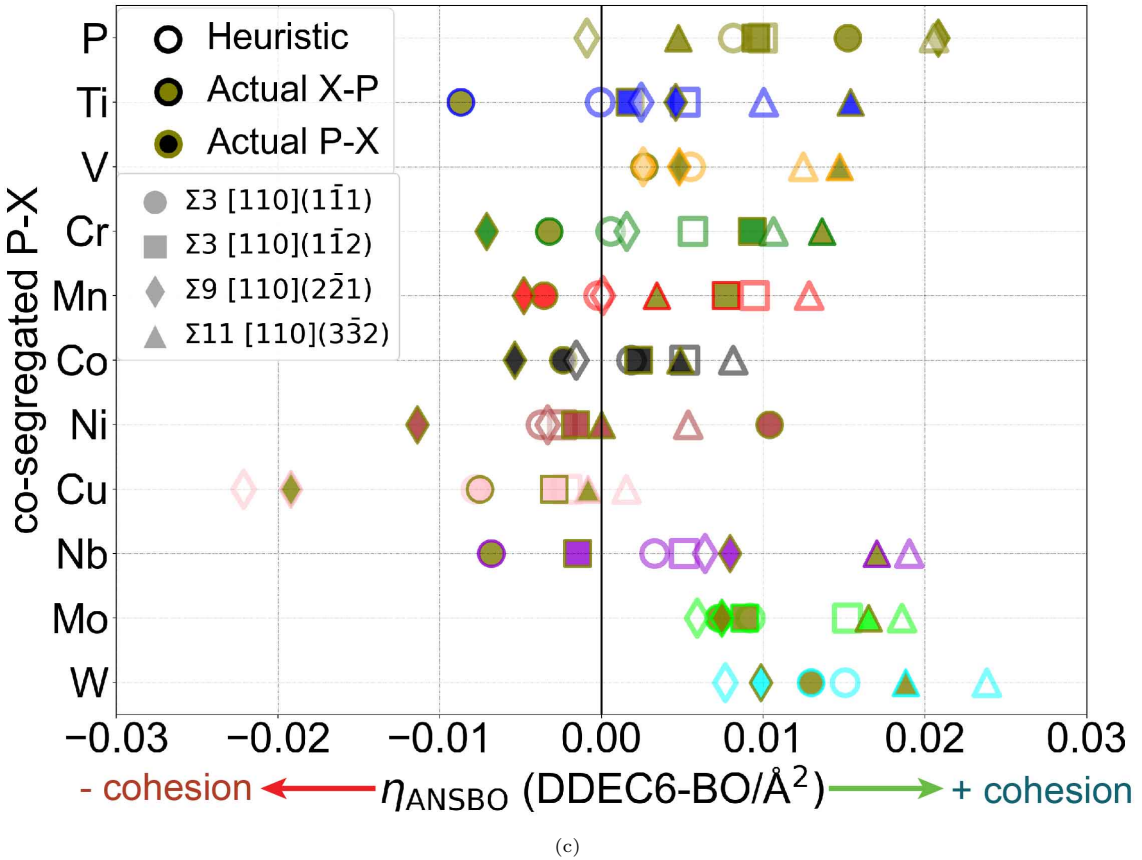


Figure S17: The cohesion effects (η), calculated in various frameworks are plotted for each co-segregating pair against the heuristic sum of each solutes' individual effects on GB cohesion. These plots show the estimated effect from the linear sum of each solute's effects with respect to the actual calculated effect of the co-segregated pair. Only the cohesion effect calculated at the most energetically favourable pair-configuration (P-X vs X-P) is shown. No data is plotted in the cases where incremental segregation of the second solute is unfavourable in both pair configurations. This comparison is generated for the S17a Rice-Thomson-Wang rigid separation framework, S17b Rice-Thomson-Wang relaxed separation framework and S17c area-normalised summed DDEC6 bond-order framework. GB-specific plots with both configurations are presented in Supplementary Figs. S14-S16. The data is presented in Supplementary Tables S18-S21.

10. Kinetics

We calculated the diffusion rates of P and the ten studied transition metals in α -Fe across the temperature range 350° C—650° C, which is the range best known to induce detrimental temper embrittlement of steels. To do so, we computed the diffusion rates via the Arrhenius diffusion equation:

$$D = D_0 e^{-\Delta Q/(k_B T)} \quad (1)$$

where D is the diffusion coefficient, D_0 is the diffusivity prefactor, ΔQ the activation energy, k_B is the Boltzmann constant, and T the temperature. We use the values calculated in Versteylen et al.’s work in [3] for ferromagnetic BCC (α) iron. We tabulate the diffusion rates calculated between 300-600° C in Table S22, and plot the diffusion rates on a logarithmic bar plot for visualisation in Fig. S18. We only provide a single plot at 400° C since the *relative* difference in diffusion speeds compared between solutes remains similar across the temperature range.

In this case, we may observe that P-diffusion is at least 1-2 orders of magnitude faster than any of the studied TMs, and thus is most likely to occupy its favoured site at the GB.

Element	Diffusion rate (m ² /s)			
	300°C	400°C	500°C	600°C
P	9.14e-27	1.37e-23	3.11e-21	2.03e-19
Ti	3.31e-28	9.80e-25	3.67e-22	3.53e-20
V	5.66e-29	2.20e-25	1.01e-22	1.14e-20
Cr	7.20e-29	2.68e-25	1.19e-22	1.30e-20
Mn	6.02e-28	1.59e-24	5.46e-22	4.93e-20
Co	2.33e-30	1.34e-26	8.22e-24	1.16e-21
Ni	1.57e-28	4.64e-25	1.74e-22	1.67e-20
Cu	5.95e-28	1.38e-24	4.33e-22	3.63e-20
Nb	2.25e-27	5.00e-24	1.51e-21	1.23e-19
Mo	2.90e-28	8.44e-25	3.12e-22	2.97e-20
W	5.14e-29	1.71e-25	6.99e-23	7.19e-21

Table S22: The solute diffusion rates in ferromagnetic α Fe, calculated using D_0 and ΔQ from Versteylen et al.’s study [3].

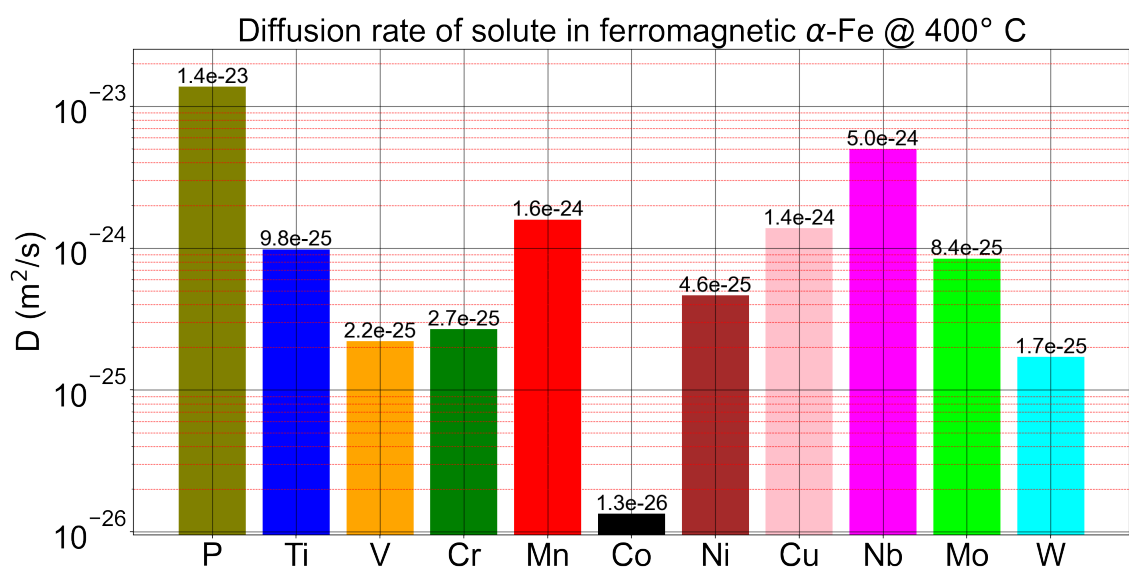


Figure S18: The solid diffusion rates of the studied elemental solutes in a Fe-X alloy, as calculated by the Arrhenius diffusion equation for the ferromagnetic α -Fe state are plotted using the data for 400°C in Table S22.

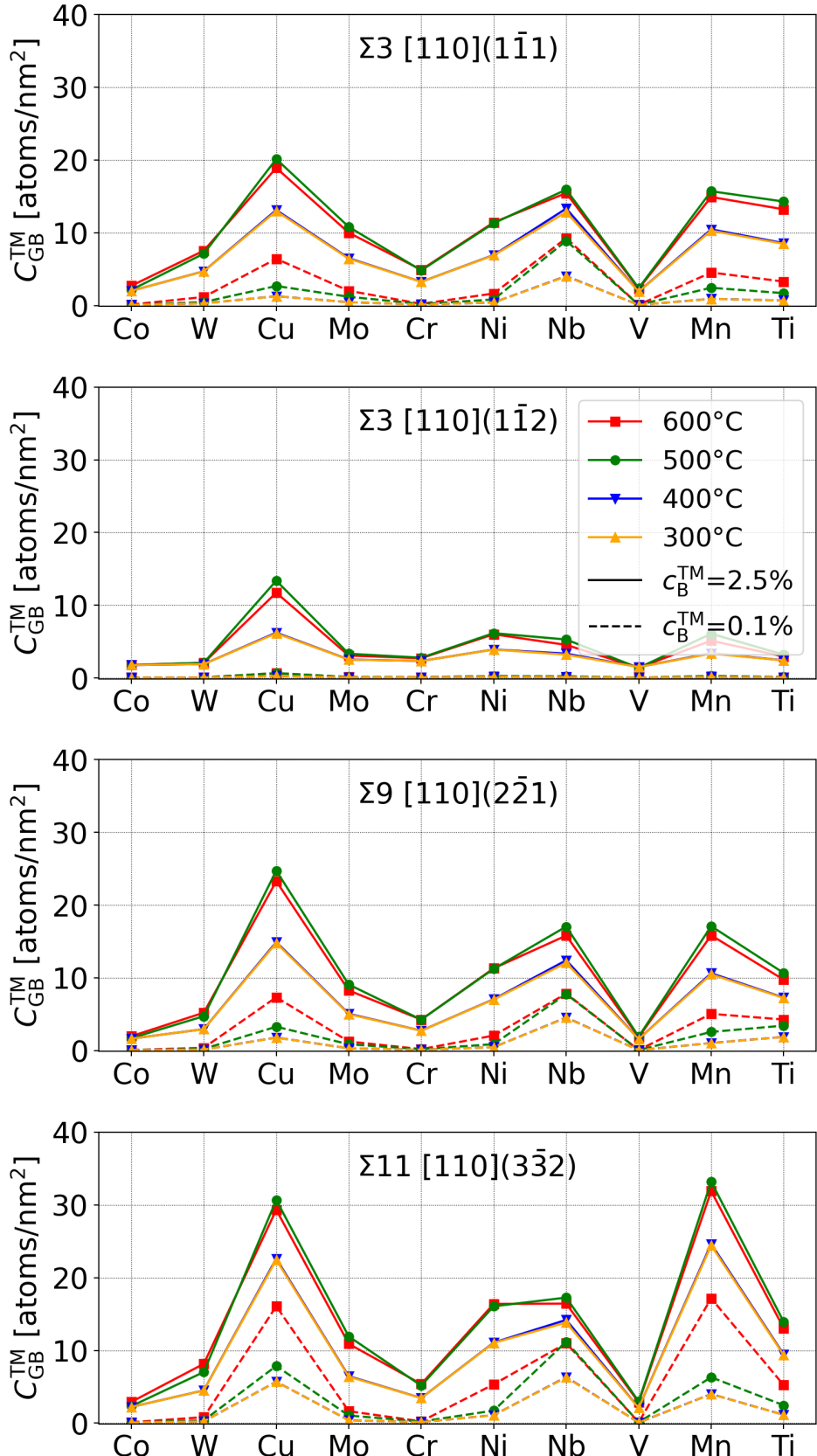


Figure S19: The final interfacial segregation coverage of TM solutes in each of the GBs at the end of each of the heat treatments simulated in this study in the binary Fe-TM case, for comparison with Fig. 11b in the main text. The heat treatments are distinguished by their different final isothermal holding temperatures of 300/400/500/600°C. c_{GB} is the coverage of the solute at the GB, and c_B is the concentration of the solute in the bulk. The compositions considered for each of the ternary alloys are: $c_B^P = 0.1$ at.% P, $c_B^{TM} = 0.1$ at.-%/2.5 at.-% TM. Note that these are upper bounds for expected observed experimental coverage (see discussion in the main text).

References

- [1] H. L. Mai, X.-Y. Cui, D. Scheiber, L. Romaner, S. P. Ringer, The segregation of transition metals to iron grain boundaries and their effects on cohesion, *Acta Materialia* 231 (2022) 117902. [doi:10.1016/j.actamat.2022.117902](https://doi.org/10.1016/j.actamat.2022.117902).
- [2] O. Gorbatov, A. Hosseinzadeh Delandar, Y. Gornostyrev, A. Ruban, P. Korzhavyi, First-principles study of interactions between substitutional solutes in bcc iron, *Journal of Nuclear Materials* 475 (2016) 140–148. [doi:10.1016/j.jnucmat.2016.04.013](https://doi.org/10.1016/j.jnucmat.2016.04.013).
- [3] C. D. Versteylen, N. H. van Dijk, M. H. F. Sluiter, First-principles analysis of solute diffusion in dilute bcc Fe-X alloys, *Physical Review B* 96 (9) (2017) 094105. [doi:10.1103/PhysRevB.96.094105](https://doi.org/10.1103/PhysRevB.96.094105).